INVITED PAPER

Design of Energy- and Cost-Efficient Massive MIMO Arrays

This paper discusses how multiuser massive microwave and mm-wave MIMO can support communications among many users over a given allocation of spectrum, along with manageable array form factors and power consumption.

By Antonio Puglielli, *Student Member IEEE*, Andrew Townley, *Student Member IEEE*, Greg LaCaille, *Student Member IEEE*, Vladimir Milovanović, Pengpeng Lu, Konstantin Trotskovsky, Amy Whitcombe, Nathan Narevsky, *Student Member IEEE*, Gregory Wright, Thomas Courtade, *Member IEEE*, Elad Alon, Borivoje Nikolić, *Senior Member IEEE*, and Ali M. Niknejad, *Fellow IEEE*

ABSTRACT | Large arrays of radios have been exploited for beamforming and null steering in both radar and communication applications, but cost and form factor limitations have precluded their use in commercial systems. This paper discusses how to build arrays that enable multiuser massive multiple-input–multiple-output (MIMO) and aggressive spatial multiplexing with many users sharing the same spectrum. The focus of the paper is the energy- and cost-efficient realization of these arrays in order to enable new applications. Distributed algorithms for beamforming are proposed, and the optimum array size is considered as a function of the performance of the receiver, transmitter, frequency synthesizer, and signal distribution within the array. The effects of errors such as phase noise and synchronization skew across the array are analyzed. The paper discusses both RF frequencies below 10 GHz, where fully digital techniques are preferred, and operation at millimeter (mm)-wave bands where a combination of digital and analog techniques are needed to keep cost and power low.

KEYWORDS | Beam nulling; beamforming; fifth-generation (5G); massive multiple-input–multiple-output (M-MIMO); millimeter (mm)-wave MIMO; mm-wave mobile networks; multiuser MIMO (MU-MIMO); next-generation (xG)

I. INTRODUCTION

To bring faster data rates to a growing number of users, the new generation of wireless systems will rely on much denser deployment of infrastructure to provide seamless connectivity. If deployed naively, these dense systems will be interference-limited; to address this, spatial directivity is being actively studied as a means to both reduce interference and increase the overall capacity. Multiple-input–multiple-output (MIMO) wireless technology takes advantage of spatial degrees of freedom through the use of multiple antennas (or multiple antenna beams, in a large array scenario) on both the transmit and the receive sides. These spatial degrees of freedom are used to both reduce the outage probability and increase the peak achievable rate in single-user systems. Performance gains in multiuser (MU) systems are even more significant since large MIMO arrays can communicate simultaneously with many users. As a result, virtually every proposal for a future commercial wireless system has studied the use of large-scale MIMO arrays. The key obstacle to scaling up the size of antenna arrays has been keeping the cost and energy consumption sufficiently low. This work examines the tradeoffs in designing such systems in a cost- and

Manuscript received July 2, 2015; revised September 14, 2015 and October 14, 2015; accepted October 14, 2015. Date of publication December 17, 2015; date of current version February 17, 2016. This work was supported by the NSF, DARPA, the UC Discovery Program, and BWRC industrial sponsors.

A. Puglielli, **A. Townley**, **G. LaCaille**, **V. Milovanović**, **P. Lu**, **K. Trotskovsky**, **A. Whitcombe**, **N. Narevsky**, **T. Courtade**, **E. Alon**, **B. Nikolić**, and **A. M. Niknejad** are with the Berkeley Wireless Research Center, University of California, Berkeley, CA 94720 USA (e-mail: niknejad@berkeley.edu).

G. Wright is with Alcatel-Lucent Bell Laboratories, Holmdel, NJ 07733 USA.

Digital Object Identifier: 10.1109/JPROC.2015.2492539

energy-constrained manner, within the contexts of both the fifth-generation (5G) cellular networks and our center's vision of a universal next-generation (xG) network.

A. xG Wireless Communication

A vision for the xG wireless network is captured in Fig. 1 [1]. Several important concepts are shown in this figure. First and foremost, a large aperture access point or xG Hub, composed of hundreds to possibly thousands of antennas and radios, provides indoor connections to a plethora of devices using highly directional beams. Because spatial selectivity avoids interference, beamforming enables spectrum reuse and simultaneous communication to many devices.

Another important concept illustrated by the figure is that the xG Hub does not need a wired connection to the backbone. Because it has a large aperture, it can form extremely narrow beams and is capable of communication over large distances (hundreds of meters to kilometers). Several xG hubs can be connected to one another in a mesh network, completely obviating the need for a wired backhaul.

In today's wireless systems, different radio standards are used to communicate with a wide variety of devices. These include LTE, WiFi, Bluetooth, Bluetooth LE, and ZigBee, as well as custom or proprietary standards. The xG hub can provide a common radio interface to support a very wide range of data rates, communication distances, bandwidths, transmit powers, sensitivities, and energy requirements. One would not expect a small, energy-starved device such as a sensor to communicate as quickly as a tablet, but nevertheless the hub should provide a lower speed radio interface that allows all the devices to communicate.

B. Fifth-Generation Mobile (5G)

5G technology is positioned to address shortcomings of existing wireless systems, including lack of interoperability between personal area (e.g., Bluetooth), local area (WiFi), and metropolitan area networks (MANs). MU-MIMO enables 5G technology to achieve higher capacity and less interference, while utilizing millimeter (mm)-wave bands increases the available spectrum. In particular, 5G is positioned for a future with "everything in the cloud"—for example, a desktop-like experience on the go, immersive experiences (lifelike media everywhere), ubiquitous connectivity (intelligent web of connected things), and telepresence (low-latency machine-to-machine communications in control loops) [2].

To capture this range of application scenarios, the following "rainbow of requirements" for mobile devices has been defined: 1) peak data rates up to 10 Gb/s; 2) cell edge data rate approaching 1 Gb/s; 3) cell spectral efficiency close to 10 bits/s/Hz; 4) mobility at speeds up to 500 km/h; 5) cost efficiency that is 10–100× better than 4G; 6) over 1M simultaneous connections per km^2; and finally, 7) a latency of 1 ms (see Fig. 2 for a comparison to 4G [2], [3]).

Interestingly, there are many elements of 5G that are still under discussion. Specific frequency band allocations, modulation schemes, power levels, and many other important factors are still being debated. Nevertheless, the goal of the 5G vision is very clear, and to date several key ideas have been proposed to address these requirements.

The xG vision and 5G vision overlap in many ways, particularly in the air interface incorporating massive MIMO below 30 GHz and mm-wave beamforming above 30 GHz. Dense deployment of wireless infrastructure requires large and possibly conformal antenna arrays whose cost needs to scale inversely with deployment density.

In this paper, we focus on the physical realization of algorithms needed to support xG and a hardware platform that supports the required signal processing given practical limits on energy and cost. Our key contributions include: 1) a distributed implementation of digital beamforming to reduce the energy required by data communication within

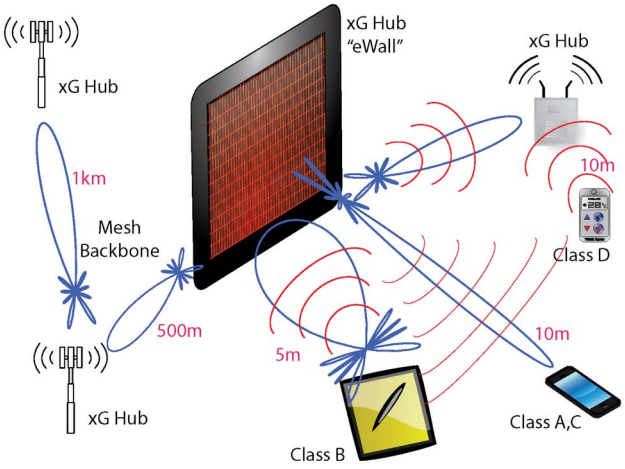

Fig. 1. *Berkeley Wireless Research Center (BWRC) xG ($x \geq 5$) vision for the Next Generation Wireless Standard.*

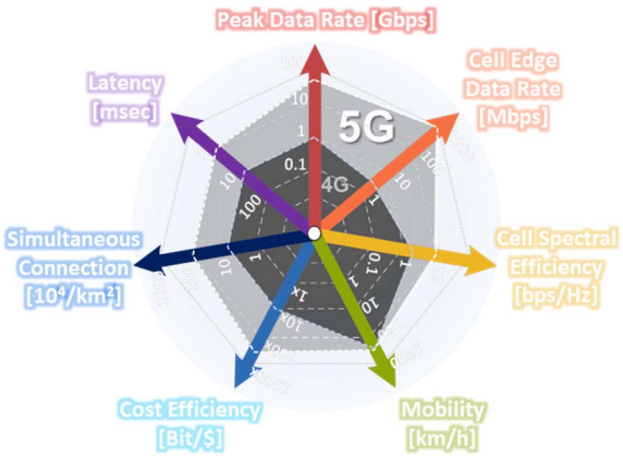

Fig. 2. *5G rainbow of requirements [3].*

the array; 2) a detailed analysis of transceiver specifications, which reveals that array averaging can be exploited to relax per-element specifications; and 3) a thorough discussion of architectures, algorithms, and hardware suitable for mm-wave applications.

II. MASSIVE MIMO TECHNOLOGY

Massive MIMO is a new and technically challenging system. Its key feature is the use of a large number of base station antennas to communicate with a much smaller number of users. Massive MIMO is therefore fundamentally multiuser in nature and makes use of generalized forms of beamforming techniques used in phased or adaptive arrays. It is under intense theoretical study, and several efforts have been made to develop prototypes validating theoretical results in practical deployment scenarios. However, no complete massive MIMO system has been built so far that simultaneously demonstrates the expected capacity increase and simplified signal processing in a realistic and cost-effective use case.

A. History and Background

MIMO has advanced rapidly over the last two decades. One reason for this is that the underlying technologies were developed well before they were fully exploited. It was known as early as the 1960s that antenna arrays could perform spatial filtering and separate signals simultaneously arriving from different directions (see [4] and references therein for an extensive review). As processing and manufacturing capabilities progressed, array processing received a surge of interest in the 1990s [5], [6] with the promise of cost-effective implementation in the area of wireless communications. The discovery of the multichannel capacity formula, furthermore, showed the enormous potential of MIMO systems [7], [8], and almost immediately, systems were built that demonstrated large capacity increases [9].

On the strength of these demonstrations, MIMO techniques were incorporated into wireless LAN standards and the 4th generation mobile network [10], [11]. Wireless LANs have had success in sending multiple data streams to a single user device ("single-user MIMO," or SU-MIMO), due in part to the fact that laptops and tablets are big enough to accommodate multiple antennas. In wide area wireless networks, where phone-sized devices predominate, SU-MIMO has limited benefits. However, since the size of the base station is not as tightly constrained, it is possible to increase the number of antennas there and utilize them for space division multiplexing (forming geometric beams) or MU-MIMO (forming generalized beams).

Even with more antennas at each base station, achieving high capacity in the wide-area wireless network remains a daunting task. Space division multiplexing is conceptually straightforward and relatively easy to implement. The system described by Avidor [12] had narrow, steered beams and intercell coordination to avoid interference. It also promised high capacity, but required prohibitively low-latency wireline connections to control the coordination between cells.

The problem of distributing data to multiple base stations also affects cooperative multipoint (CoMP), a MIMO technique that relies on multiple base stations communicating to a single user terminal. While CoMP has been part of the LTE standard since release 8 [13], wider adoption may have to wait for "cloud radio access networks" (C-RANs), where virtual base stations reside in a common data center, since CoMP requires very fast data transfer between base stations.

Massive MIMO, inspired by Marzetta [14], promises to greatly improve capacity without requiring the overwhelming complexity of intercell coordination. In brief, Marzetta observed that as the number of base station antennas becomes much larger than the number of user terminals, it is possible to form (generalized) beams such that there is almost always only a single user in each beam [14], thereby giving each user their own interference-free, high-capacity link to the base station. In this limit, the probability that a beam points toward a neighboring base station becomes vanishingly small as well, and intercell interference approaches zero without coordination between cells. This promise of simplified deployment is one of the most attractive aspects of massive MIMO.

While it is always true that with enough base-station antennas one can get at most one user per beam (the "pseudo-orthogonality" condition), determining just how many antennas is enough is of great practical importance. There is experimental evidence, discussed below, that this is on the order of 100 elements to support an order of magnitude fewer user terminals [15]–[17].

B. mm-Waves Versus RF

Operation at mm-wave frequencies is attractive because an array with a large number of antennas is physically small. Simulations of mm-wave massive MIMO systems show promise of large capacity [18]. Measurements of propagation in the low mm-bands are also encouraging [19]. However, while mm-wave systems can achieve high gain with physically small antennas, mobility management—initial synchronization, registration, paging, and handoff of mobile terminals—can require signals that are broadcast throughout a sector. The system-level tradeoffs needed to maximize the use of the narrow, high-gain beams are an open research question.

In this paper, we will make an artificial distinction between RF and mm-wave frequencies. For the purpose of this paper, mm-waves are defined as carrier frequencies above 30 GHz. For RF frequencies, particularly below 10 GHz, we propose a fully digital and distributed array architecture, while at higher frequencies, we propose a hybrid architecture using both analog and digital beamforming. Because each antenna is small at mm-wave frequencies,

one can easily build an array with an order of magnitude more elements than at RF. However, providing a complete digital radio for every single element is cost- and energy-prohibitive. Instead, a group of elements can be combined to form an analog subarray, using analog processing of amplitude and phase to create an arbitrary antenna pattern (for example, tapering to reduce sidelobes). These subarrays can then be used in a variety of ways, such as sectorizing the cell, assigning each subarray to a single user, or utilizing lower-dimensional digital beamforming.

C. Massive MIMO Testbeds

The promise of system benefits from deploying massive MIMO, coupled with the uncertainties of channel propagation characteristics and practical hardware design issues, has led to several demonstration projects ranging from large-scale simulations to actual hardware. Measurements have studied channel estimation and beamforming performance at low and mm-wave frequencies, while system simulations have generally attempted to quantify the performance of massive MIMO in outdoor environments with moving users. In 2011, the GreenTouch consortium demonstrated a 16-element array "Large-scale antenna system (LSAS)" [20] in which a software radio implemented a channel estimation algorithm and computed beamforming weights. The main result of the study was that the effective antenna gain increased linearly with the number of antennas, both in ideal (anechoic chamber) and real indoor (scattering) environments. This allowed the radiated transmit power per element to be reduced proportionally, which was the goal of the demonstration.

The Ngara system built by CSIRO in Australia [21]–[23] implements an array of up to 32 antennas operating at UHF for multiuser communications. This system is structured as a cascade of modules, with a bank of field-programmable gate arrays (FPGAs) performing all the baseband processing and connecting to 32 data converters. The RF/analog circuits are divided into two modules with analog signals routed between them. Ngara has demonstrated 50 Mb/s uplink and downlink rates to all users over 28 MHz bandwidth, including online processing of 14 user streams in the uplink, achieving a spectral efficiency up to 67 bits/s/Hz. The recently proposed USC SDR [24] system is assembled hierarchically using servers, FPGAs, and custom-designed RFICs. One or more servers control a series of FPGAs, each of which is connected to up to four radios. The backplane is designed using high-speed PCIe interfaces to perform fully centralized processing on the servers. The system is being used for MIMO experiments.

The Argos [25] and ArgosV2 [26] projects are systems with 64 and 96 antennas, respectively, operating in the 2.4-GHz ISM band. They are designed in a hierarchical manner, with a central controller serving several hubs, each of which connects to a number of radio modules and provides both a backhaul connection as well as digital signal processing capability through a local FPGA. The 64-element Argos system has achieved a capacity up to 80 bits/s/Hz serving 15 users [25]. The radio modules are connected to FPGA boards to enable local signal processing within the array; the FPGA boards are then connected to a central computer and further signal processing is done offline using MATLAB. Argos has demonstrated that there is no penalty in doing conjugate beamforming in a distributed manner. This is an important result since conjugate beamforming (discussed in Section III) is computationally simple and doing the processing locally within the array reduces intra-array data transfer. However, the Argos data also shows that significantly higher capacity can be attained by using zero-forcing instead of conjugate beamforming, in contrast with the theoretical expectations [27].

The LuMaMi system at Lund University [28] is a 100-element array that communicates with 10 users over a 20-MHz channel at 2.6 GHz. The system uses 50 FPGAs to implement the baseband processing after data aggregation. The baseband samples are communicated to the FPGAs and the central processor over a hierarchical backhaul network that achieved an aggregate throughput of 384 G using a series of interconnected PCI Express interfaces and serializers. Preliminary results indicate that this system is capable of uplink spatial multiplexing [28], [29]. Gao *et al.* took channel measurements at 2.6 GHz using a 128-element array [15], [29] and empirically observed that the pseudo-orthogonality of users' channels promised by the theory of massive MIMO [14] does indeed emerge in real propagation environments.

D. Practical Deployment Issues

Large-scale arrays have been studied for a variety of applications, ranging from extending the reach of wireless backhaul links (e.g., [21], [30], and [31]) to reducing interference in cellular and local-area networks. The focus of current interest is the study of deploying massive MIMO systems for 5G cellular networks [32]. For example, Huh *et al.* [33] have studied how massive MIMO techniques can be adopted while reusing as much of the existing LTE standard as possible.

Some of the LTE bands support time-division duplexing (TDD), but most LTE deployments use frequency-division duplexing (FDD). In a TDD system, since the uplink and downlink frequencies are the same, the uplink channel state information (CSI) can be used in the downlink as well. In contrast, FDD massive MIMO requires separate uplink and downlink channel estimation. In the worst case, the user terminal may be required to estimate and feed back CSI for every antenna at the base station. An FDD massive MIMO system may need to use a significant fraction of its overall capacity just for CSI acquisition and feedback. However, there is reason to expect that the downlink channels from each base-station antenna element are correlated, providing an opportunity to reduce the amount of channel sounding. Researchers from Samsung have simulated a three-dimensional channel

model with a non-line-of-sight (non-LOS) path and an FDD channel separation of 45 MHz [34]–[36], finding that the capacities of the up- and downlinks were highly correlated. Variations in direction of arrival of about 15° were common, though the misalignment was less than 30° 99.6% of the time. These results suggest that the uplink direction of arrival can be used as a start for an iterative downlink channel estimation scheme, though this needs to be verified experimentally. However, wider FDD duplex spacing will reduce the correlation between the up- and downlink channels [37], [38], and FDD channel estimation remains an open research question.

Another unresolved question relates to network management in a massive MIMO system. The network needs to be able to efficiently perform user registration, paging, and handoff even if a highly directional link has not yet been established. This task is complicated by the fact that, before CSI is acquired, the control channel signal-to-interference-plus-noise ratio (SINR) is very low due to the lack of array gain. Network management functions may require the use of broadcast signals, followed by establishing a directional connection to the user from scratch. As such, they may impose significant overhead on massive MIMO systems. A related problem is user mobility; it is unknown how robust massive MIMO is to high user speeds or how well beams can be steered to track the user's location.

In summary, massive MIMO demonstrations so far have shown that with slowly moving mobile terminals and TDD: 1) channel estimation can be done well enough to allow the antenna gain to grow linearly with the number of elements; 2) centralized beamforming can reach the expected capacity; and 3) distributed beamforming schemes are feasible, although their ultimate performance is not yet known. However, there are many outstanding questions relating to efficient and optimized implementations. In particular, since massive MIMO requires many more RF transmit and receive chains than current base stations, questions of cost are of prime importance.

III. BEAMFORMING AND BEAM NULLING

The key signal processing techniques for directional communication are beamforming and nulling. We consider first narrowband communication (where the multipath delay and the propagation time of a wavefront across the array aperture are small relative to the symbol period) over a TDD channel. The propagation from a user terminal or other signal source to an array with M elements can be described in terms of the $M \times 1$ channel vector h. For example, for a uniform linear array (ULA) with a signal impinging at an angle of ϕ from broadside

$$h = \begin{bmatrix} 1 & e^{j\theta} & e^{j2\theta} & \dots & e^{j(M-1)\theta} \end{bmatrix}^T \tag{1}$$

where $\theta = kd\sin(\phi)$, k is the wave-vector and d is the spacing between elements. Environments with more complicated propagation characteristics, such as multipath, diffraction, and shadowing, have more complicated channel vectors. Because the channel is TDD, transmit and receive propagation are reciprocal,[1] and the channel vector for transmission from the array to the user is h^T.

In a multiuser scenario with K users, this description can be extended to an $M \times K$ channel matrix H. In receive (uplink) mode, if users transmit signals s, the array receives

$$r_{\text{array}} = Hs + n_M. \tag{2}$$

Here, n is a vector of independent identically distributed (i.i.d.) white Gaussian noise with variance σ_c^2. In transmit (downlink) mode, if x is the vector of signals at each antenna, the users receive

$$r_{\text{user}} = H^T x + n_K. \tag{3}$$

Receive or transmit beamforming consists of applying a linear transformation to convert between user data streams and antenna waveforms. These operations are performed by $K \times M$ receive beamforming matrix G_{rx} and $M \times K$ transmit beamforming matrix G_{tx}. The complete signal model is

$$\hat{s}_{\text{array}} = G_{\text{rx}} Hs + G_{\text{rx}} n_M \tag{4}$$

$$\hat{y}_{\text{user}} = H^T G_{\text{tx}} y + n_K \tag{5}$$

where s and y are the uplink and downlink user symbols, respectively.

If the channel matrix is known at the array, the beamforming weights can be computed in closed form for a given objective function. Two common algorithms are conjugate beamforming, which maximizes signal-to-noise-ratio (SNR), and zero-forcing (ZF) beamforming, which nulls interuser interference. In the receive direction, these are given by

$$\begin{aligned} G_{\text{c}} &= H^H \\ G_{\text{zf}} &= \left(H^H H\right)^{-1} H^H \end{aligned} \tag{6}$$

where the superscript ^{H} denotes the Hermitian transpose. In the transmit direction, because of reciprocity, $G_{\text{tx}} = G_{\text{rx}}^T$.

[1]Transmit–receive reciprocity holds true only for the propagation environment. Since the analog front ends are subject to random gain and phase errors, they contribute a nonreciprocal portion to the channel. Generally, this is compensated by an appropriate calibration algorithm; see [25] for an algorithm and implementation results.

Consider the line-of-sight (LOS) channel described in (1). It can easily be seen that the conjugate beamforming vector is

$$g_c = \begin{bmatrix} 1 & e^{-j\theta} & e^{-j2\theta} & \dots & e^{-j(M-1)\theta} \end{bmatrix}^T \tag{7}$$

which gives the well-known phased array coefficients. From this, we see that conjugate beamforming places the peak of the array radiation pattern in the direction of the given user, with no consideration of interuser interference. ZF beamforming instead applies the constraint of placing nulls in the directions of all other users. This eliminates multiuser interference but often results in a lower gain main lobe of the antenna pattern. An illustrative comparison of conjugate and zero-forcing patterns is shown in Fig. 3 for the case of an eight-element array serving three users. In exchange for precisely placing nulls in certain directions, ZF beamforming reduces the gain in the main lobe and leads to a generally higher sidelobe level. More generally, these tools—placing peaks and nulls in the radiation pattern—are the key ingredients of beamforming, and different objective functions result in different overall radiation patterns.

A. Wideband Beamforming

When the signal bandwidth becomes large, it is not possible to neglect time delays caused by propagation through the channel. There are two main effects to consider. First, multipath components propagate along different physical paths in the environment with different path delays. Second, for very large arrays or very wide bandwidths, the propagation delay of a wavefront across the array aperture cannot be neglected. In radar systems, the latter effect is compensated by true-time delay (TTD) beamforming that aligns the signals in time at each element in addition to correcting the path-length-dependent phase shift.

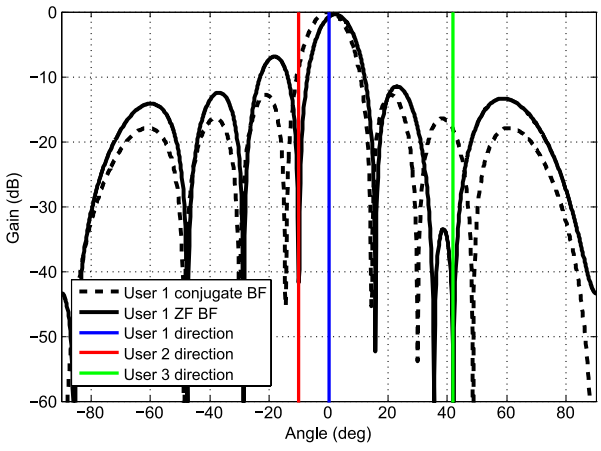

Fig. 3. *Comparison of conjugate and ZF radiation patterns for an eight-element array serving three users with distinct directions of arrival. Only the radiation patterns for the first user are shown.*

One of the advantages of orthogonal frequency division multiplexing (OFDM) modulation is that it decomposes a wideband channel into many parallel, narrowband orthogonal subchannels. This is done by modulating data symbols onto a discrete Fourier transform (DFT) basis of dimension N_{sc}. Each of these narrowband subcarriers $l \in [1, N_{sc}]$ propagates through a corresponding channel matrix H_l. Therefore, beamforming matrices can be obtained independently for each subcarrier using the methodology described above (this technique has been demonstrated by [21] and [28]). This signal processing technique results in an array pattern that varies with frequency. Intuitively, frequency-domain beamforming both matches the radiation pattern to the frequency-dependent propagation environment and performs an interpolation that aligns the delayed signals in time.

At mm-wave, OFDM frequency-domain beamforming is a less promising architecture due to its incompatibility with analog or hybrid beamforming as well as undesirable characteristics of OFDM (such as high peak-to-average-power ratio). At these frequencies, wideband beamforming is performed using TTD elements, which corrects only for the propagation time across the array aperture. Analog, time-domain beamforming techniques that respond to the multipath characteristics of the channel are an open research question.

B. Channel Estimation

In order to design beamforming matrices, the array needs to have an estimate of the channel matrix. For a TDD system, by exploiting reciprocity, this can be estimated in the uplink [14], [32], [39]–[41]. As discussed in Section II-A, the users are assigned orthogonal pilot sequences that they transmit to the array; this enables estimation of an entire column of H with one pilot resource. The channel estimation overhead of a TDD system is therefore proportional to K.

An additional consideration in channel estimation is whether the beamforming is performed centrally or in distributed fashion. Since each element has access to its own row of H, from (6) conjugate beamforming can be performed in distributed manner at each element [25]. On the other hand, zero-forcing requires inversion of the matrix $H^H H$; consequently, at least the matrix inversion must be performed centrally.

C. Distributed Phase Rotation

We now consider *how* phase rotation is implemented in the array, comparing centralized and distributed approaches. Distributed rotation refers to the case where beamforming weights are applied locally at each antenna. Centralized phase rotation refers to the case where the beamforming signal processing is performed at a central location (e.g., the main system controller). This distinction is valid only for a digital implementation, where conversion between analog and digital domains and phase

rotation can take place very far away from each other. In contrast, analog phase rotation is fundamentally distributed since the beamforming functionality is embedded directly into the transceiver and the signal routing network. The analysis in the rest of this section therefore assumes a digital beamforming and routing scheme.

Centralized phase rotation fundamentally requires I/O bandwidth at the central processor prorportional to M. In the receive direction, each antenna forwards its digitized waveform to the central processor, where the signals are combined to generate the users' data streams. In the transmit direction, the M unique waveforms are generated at the central processor and then forwarded to the appropriate antenna. In both of these cases, data enters or exits the central processor at the rate

$$R_{\text{centr}} = 2MN_{\text{bit,adc}}f_{\text{s}} \tag{8}$$

where $N_{\text{bit,adc}}$ and f_{s} refer to the bitwidth and sampling rate, respectively, of the analog-to-digital or digital-to-analog converters (ADC/DAC). In massive MIMO base stations, where M is expected to be between 100 and 10 000, this scaling is undesirable. The required backhaul capacity is a substantial cost, both in hardware and power. In fact, recent prototypes have encountered the backhaul bottleneck and had to invest considerable engineering effort and expense to mitigate it [28], [42], [43].

The solution to this problem is to perform phase rotation in a distributed manner [25], [44]. The key insight is that the M waveforms at the array antennas are not linearly independent, but instead lie in a K-dimensional subspace generated by the K distinct users. Exploiting this redundancy, it is possible to exchange K rather than M unique signals with the central processor by performing distributed phase rotation. In the massive MIMO regime, where $M \gg K$, the required backhaul capacity is substantially reduced.

Since linear beamforming is simply a matrix multiplication, this computation can be easily distributed. When receiving, each element multiplies its received signal by its column of G_{rx}, generating a $K \times 1$ vector of user estimates. These vectors are then summed across the array, *as the signal propagates to the central processor*, to generate the per-user spatially filtered signals (Fig. 4). This task can be embedded in an interelement digital link where it is very low-latency and low-energy. When transmitting, each element receives the vector of user data streams y and generates its transmit signal by processing it with its row of the beamforming matrix G_{tx}. In an OFDM-based system, this process is repeated independently on each subcarrier. With this scheme, it can be seen that data enters or exits the central processor at the rate

$$R_{\text{distr}} = 2KN_{\text{bit,user}}B \tag{9}$$

where $N_{\text{bit,user}}$ and B are the bit width of the user signals and the channel bandwidth, respectively.

Fig. 5 illustrates the benefit of distributed phase rotation for an example case with $B = 100$ MHz, $N_{\text{bit,adc}} = 10$, and $N_{\text{bit,user}} = 15$. Maintaining a constant ratio of base station

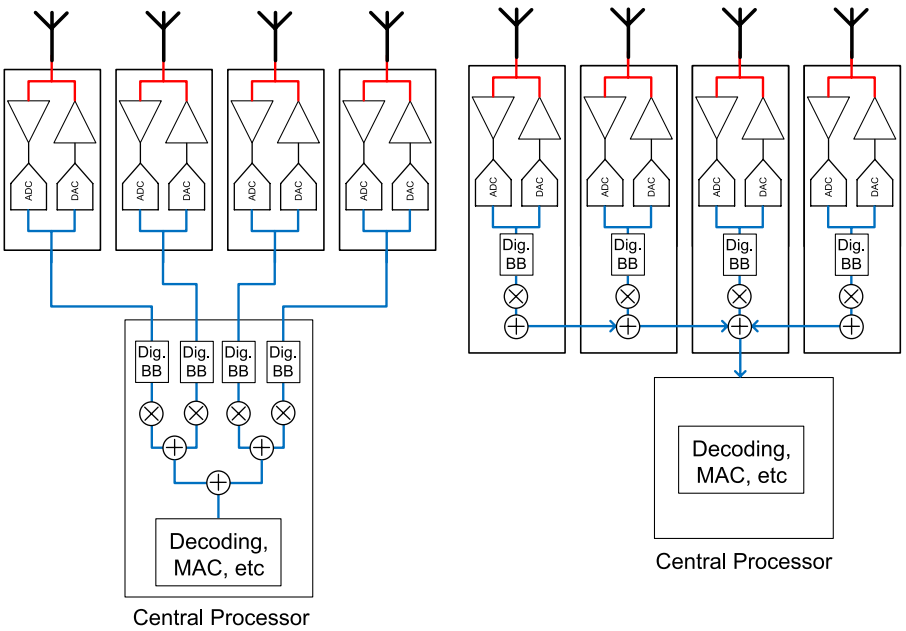

Fig. 4. *Comparison of (left) centralized and (right) distributed receive beamforming for a four-element array.*

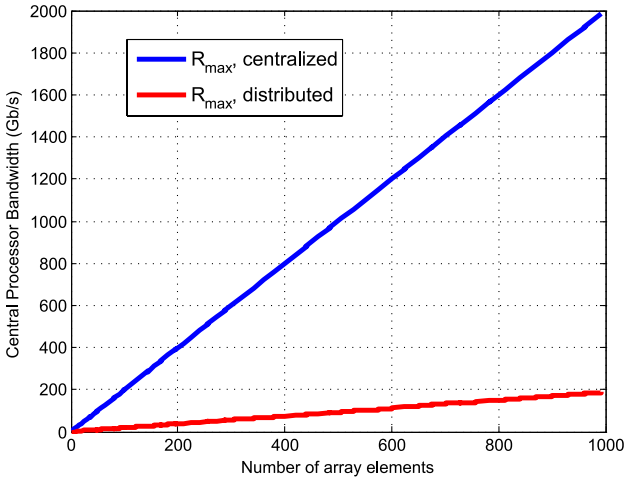

Fig. 5. *Maximum data rates using either centralized or distributed beamforming. In this example, $B = 100$ MHz, $N_{\text{bit,adc}} = 10$, and $N_{\text{bit,user}} = 15$. The number of users grows with the size of the base station with fixed ratio $M/K = 16$.*

antennas to users ($M/K = 16$), the I/O bandwidth at the central processor can be reduced by an order of magnitude by performing distributed phase rotation.

IV. ARRAY DESIGN

Energy-efficient operation of a large antenna array is simplified by the fact that performance specifications of individual transceiver elements can be relaxed while still maintaining adequate array-level performance. This leads to lower power consumption per transceiver element, which can reduce the overall energy consumption of the entire array. The quantitative reasoning behind this approach is described in the following sections and is largely motivated by the discussion in [45].

A. Tx Element Design

Arrays can greatly improve radiated power efficiency, exploiting high directivity to reduce the actual power required to deliver a certain equivalent isotropic radiated power (EIRP) [20], [21]. Because the radiation from different antennas sums in field amplitude, EIRP increases by a factor of M^2 when the number of antennas is scaled by M. Nevertheless, adding elements to the array comes with a fixed per-element overhead that does not depend on the transmit power. As a result, a portion of the system power increases with the total number of transceiver elements, implying that there exists an array size that minimizes total power consumption.

Another important consideration in large array design is the number of transceivers per IC. The simplest option is to drive each antenna with its own transceiver chip. Since each transceiver also requires support circuits such as frequency synthesis and interchip data links, equipping every single transceiver with independent copies of these blocks introduces a large amount of redundancy. Instead, multiple transceivers can be fused into one *common module* equipped with several RF chains, ADCs, and DACs and a single set of support hardware. An example of such an architecture is illustrated in Fig. 6. The number of antennas per module can also be optimized, allowing for improved energy efficiency at the system level.

To formulate the power optimization problem, we follow a procedure similar to the one in [45], considering the case where M transceivers are divided among N modules (so each module serves M/N elements). In the downlink, the total power consumption of the array can be split into three contributions

$$P_{\text{tot}} = \frac{EIRP}{M\eta} e^{\frac{\alpha\lambda}{2}\sqrt{\frac{M}{N}}} + MP_{\text{tx}} + NP_{\text{mod}}. \tag{10}$$

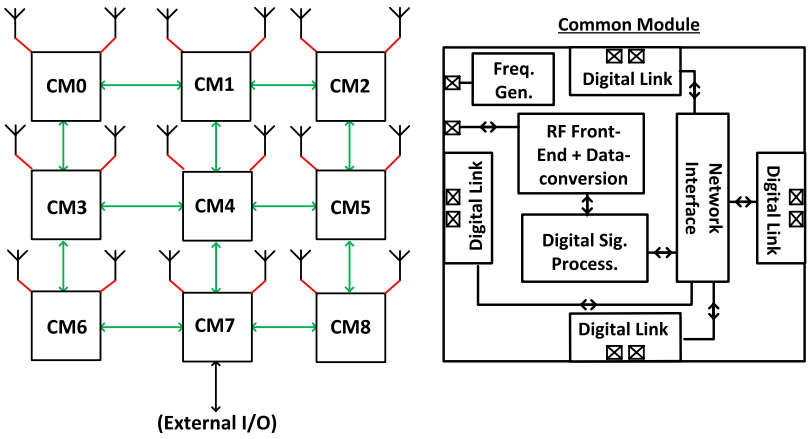

Fig. 6. *Example array composed of common modules for $M = 18$ and $N = 9$. The module block diagram shows the transceivers as well as the major shared blocks.*

The first term accounts for the radiated power, where the M isotropic transmitters each radiate a power of $EIRP/M^2$ with efficiency η and a routing loss. The routing loss is modeled assuming that each module's M/N antennas are arranged in a square with half-wavelength separation and, for simplicity, that all wires are of the same length. The loss per unit length, α, depends on the substrate, the transmission line material, and carrier frequency. The second term accounts for the fixed power consumption of each transmitter, which is independent of its radiated power. The final contribution consists of the overhead power per module, arising from blocks such as voltage regulation, frequency synthesis, and backhaul, which are shared among M/N elements.

As can be seen from (10), there are optimum values for both N and M. The optimum value for N represents the tradeoff between analog loss and sharing of functions within a common module, while the optimum value for M represents the tradeoff between radiated power and all sources of overhead. The per-element overhead is therefore the limiting factor to the achievable transmit mode power consumption.

Fig. 7 shows the array power consumption as a function of the number of elements. Each curve corresponds to a different per-transmitter power overhead P_{tx}. As expected, reducing P_{tx} reduces the power consumption of the array, increases the optimum number of elements, and flattens out the power consumption as a function of array size. Fig. 8 shows the array power consumption as a function of the number of elements per module, for constant total array size and PA efficiency. Increasing the overhead power consumption of the module increases the optimum number of RF chains per module.

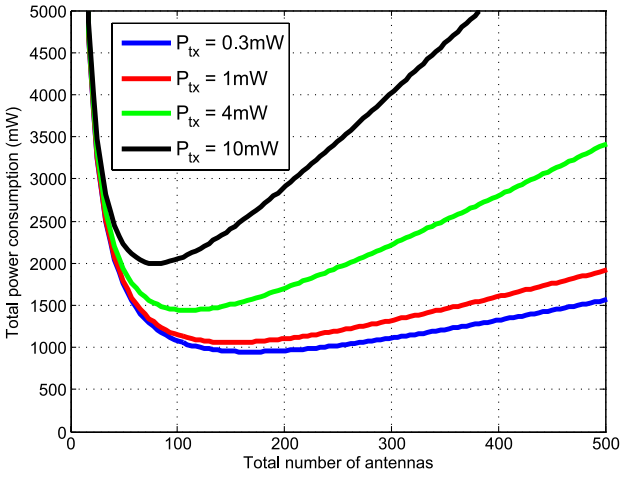

Fig. 7. ***Total array power consumption as a function of number of elements, for EIRP of 5 W and 20% transmitter efficiency. Per-element overhead is held constant at 1 mW, and the number of elements per module is held constant at 4.***

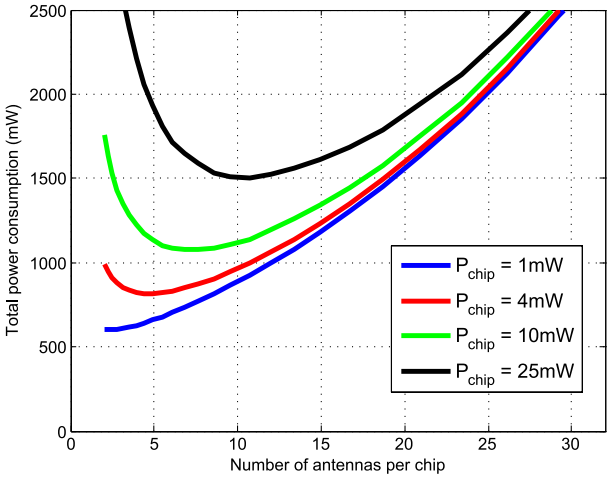

Fig. 8. ***Total array power consumption as a function of number of elements per module for 5 W EIRP and 20% transmitter efficiency. Per-transmitter overhead is held constant at 1 mW and the total array size is fixed at 256 elements.***

This analysis has considered the case where perfect channel information is available, which allows transmit power to be reduced inversely proportionally to the number of antenna elements. In the case of imperfect channel information, it has been shown that the transmit power can be reduced as $1/\sqrt{M}$ while maintaining constant capacity [46]. Though this affects the precise value of the optimum, it does not change the qualitative result. To summarize, when designing an array, each element may have substantially reduced output power compared to a single-element transmitter. However, the system must be carefully designed to minimize all sources of overhead power, as these fundamentally set a floor on the achievable system-level power consumption.

B. Rx Element Design

In the receive direction, the analysis is somewhat different. Like in the transmit direction, the array provides a signal energy gain of M^2. The receive array gain can be modeled by adding uncorrelated channel noise at the antenna of every element.[2] In addition, each element adds its own uncorrelated circuit thermal noise. Consider a reference receiver that consumes power P_{rx} to achieve desired SNR $\rho = E_{\text{s}}/(\sigma_{\text{c}}^2 + \sigma_{\text{rx}}^2)$, where the environment

[2]An exact treatment of environmental noise is very involved. If the environment can be modeled as presenting an isotropic noise temperature T_{env}, then an M-element array provides an SNR gain proportional to M. This topic is well discussed in [47]–[49]. Intuitively, though the peak array gain scales as M^2, the beamwidth scales as $1/M$, giving a net noise gain of M. At the same time, if the signal source lies fully within the beam, the signal experiences a gain of M^2. This result can be equivalently modeled by assuming that each element picks up uncorrelated noise at temperature T_{env}, giving the same SNR gain of M.

and receiver noises have variance σ_c^2 and σ_{rx}^2, respectively. An array of M such receivers achieves SNR

$$SNR = \frac{M^2 E_s}{M\sigma_c^2 + M\sigma_{rx}^2} = \frac{M\frac{E_s}{\sigma_c^2}}{1+\frac{\sigma_{rx}^2}{\sigma_c^2}}. \quad (11)$$

This expression gives a simple model for the receive array: an AWGN channel with SNR E_s/σ_c^2, followed by an array gain of M and a receiver with noise figure $NF_{arr} = NF_{elem} = 1 + (\sigma_{rx}^2/\sigma_c^2)$. Two distinct regimes of operation can be identified:

1) *Link-budget limited regime*: If the array gain is needed to achieve the desired link budget, then it comes at a cost of an M-fold increase in receiver power consumption.
2) *Non-noise-limited regime*: If a single-element receiver is able to achieve the desired link budget, then the array gain is superfluous. In this regime, it is possible to trade off array noise figure for power consumption. The noise variance of each element can be *deliberately* degraded proportionally to M (in effect undoing the array gain) in exchange for a reduction in receiver power consumption. In this case, the SNR is $M^2E_s/\left(M\sigma_c^2 + M^2\sigma_{rx}^2\right) \approx \rho$, while the power consumption is approximately only P_{rx}.

One can expect that mm-wave systems will generally operate in the link-budget limited regime, while RF arrays can operate in the non-noise-dominated regime since they can avail themselves of greater transmit power. As before, there is also an overhead power contributed by every element that should be carefully minimized. However, the key observation is that in the receive direction, there is no optimum array size since the array and element noise figures are the same. Instead, there is a noise figure–power consumption tradeoff curve, and the overall achievable power consumption is determined by the available link budget margin.

Unlike circuit thermal noise, it is possible for the ADC quantization noise to be correlated between elements if the signal power is too large relative to the noise floor. Fig. 9 illustrates this issue by showing the total SNR of an array with M elements as a function of the SNR at the input of each element's ADC. Seven bits of quantization are used in this example. For a standalone receiver $(M = 1)$, the output SNR follows the input SNR until it becomes quantization-noise-limited. As M increases, the array gain is only maintained if the random noise generated by each receiver element can be adequately resolved by the ADC. As the per-element input SNR increases, the array-level SNR becomes limited by the quantization noise of the ADC, resulting in a maximum achievable array SNR that depends upon the number of physical ADC bits.[3]

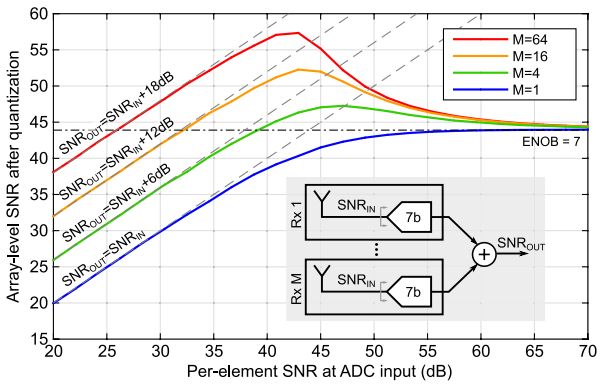

Fig. 9. ***Array-level SNR*** $(\mathrm{SNR_{OUT}})$ ***versus per-element SNR prior to 7-bit ADC quantization*** $(\mathrm{SNR_{IN}})$***. The dashed gray lines show the ideal array-level SNR assuming no quantization, and the black dashed line marks the SNR corresponding to 7 effective bits.***

C. Synchronization Requirements

Proper synchronization between array elements is necessary to obtain the performance promised by massive MIMO. Synchronization errors may lead to systematic errors that do not average out with the array size and therefore lead to signal energy degradation and multiuser interference. There are four main types of synchronization errors:

1) Carrier frequency offset (CFO): mismatches in the local oscillator (LO) frequency at each element.
2) Carrier phase offset: mismatches in the phase of the LO at each element. This can be divided into a static or slowly drifting component (relative to the frame length) and a fast-varying component (phase noise).
3) Sampling frequency offset (SFO): mismatches in the sampling frequency of the ADC or DAC at each element.
4) Sampling phase offset: mismatches in the phase of the sampling clock at each ADC or DAC. This also can be divided into a static or slowly-varying component plus fast-varying sampling jitter.

These effects can be modeled as follows. Denote the LO frequency, LO phase, and sampling instants at element i and baseband sample n as $f_{c,i}$, ϕ_{in}, and τ_{in}, respectively. Then

$$f_{c,i} = f_c + \Delta f_{c,i} \quad (12)$$
$$\phi_{in} = \phi_i + \Delta\phi_{in} \quad (13)$$
$$\tau_{in} = nT_s + n\Delta T_{s,i} + \tau_i + \Delta\tau_{in}. \quad (14)$$

[3]There are techniques to deliberately randomize quantization noise in ADC arrays by, for example, introducing known voltage or phase dither and correcting for it digitally. See [50] for a thorough overview.

Here f_c is the true channel center frequency, $\Delta f_{c,i}$ is the CFO, ϕ_i is the static LO phase for one frame, T_s is the true sampling period, $\Delta T_{s,i}$ is the sampling period error, and τ_i is the static sampling phase offset at element i for one frame. $\Delta\phi_{in}$ and $\Delta\tau_{in}$ describe a time series of the LO phase noise and the sampling jitter at the nth baseband sample.

Consider the receive direction, where element i receives $r_i[n]$ or $r_i(t)$ in discrete or continuous time. (The transmit case is identical, replacing $r_i(t)$ with the precoded symbol $x_i(t)$, with the caveat that it is generally more difficult to estimate and track frequency or phase.) Then the sampled, baseband-equivalent signal at element i is

$$\begin{aligned} r_i[n] &= e^{j\Delta f_{c,i}\tau_{in}} e^{j(\phi_i+\Delta\phi_{in})} r_i(t) \times q(t) \\ &\approx e^{j\Delta f_{c,i} nT_s} e^{j(\phi_i+\Delta\phi_{in})} r_i(t) \times q(t) \end{aligned} \tag{15}$$

where $q(t) = \sum_{n=-\infty}^{\infty} \delta(t - \tau_{in})$ is the sampling waveform of Dirac impulses. We now consider successively each error, its effect on system performance, and how to correct it.

1) CFO and SFO: The CFO at each antenna effectively contributes a random, time-dependent phase shift that is different for each element. After beamforming, this causes a loss in signal energy due to partially out-of-phase summation. At the same time, SFO at each element creates time-varying intersymbol interference (ISI) after beamforming since samples from different time instants will be summed together.

Based on this discussion, if the CFO and SFO across the array are independent, each element must have a separate carrier frequency and sampling frequency tracking loop. This can be avoided by distributing a common low-frequency reference, with each element using a phase locked loop (PLL) to generate the LO and sampling clock. This guarantees that all elements have identical LO and sampling frequencies. There may still be a global carrier frequency and/or sampling frequency offset relative to the users, but these can be estimated and tracked at the array level.

2) Static LO or Sampling Phase Offset: Now consider the per-frame static LO and sampling phase offsets ϕ_i and τ_i. Even with a common frequency reference, there will be phase offsets between the clocks at each element due to effects like routing skew. Uncorrected, ϕ_i and τ_i will contribute static signal energy degradation and ISI, respectively, analogous to the CFO and SFO. However, the key observation is that since these errors are constant over one frame, the same errors are present during the channel training phase. Consequently, the array cannot distinguish these effects from the channel phase and propagation delay and will naturally include these quantities as part of the channel estimate. Any narrowband beamforming algorithm will automatically calibrate LO phase skew; a wideband beamforming technique such as TTD or OFDM beamforming will additionally calibrate the ADC and DAC sampling skew. Only if wideband beamforming is not employed does sampling skew need to be handled at the circuit level.

3) Phase Noise and Sampling Jitter: Correcting the CFO, SFO, and static phase errors, the received signal model from (15) becomes

$$\begin{aligned} r[n] &= e^{j\Delta\phi_{in}} r_i(t) \times q(t) \\ &\approx e^{j\Delta\phi_{in}} r_i[n] \left(1 - \frac{dr_i}{dt}(nT_s)\Delta\tau_{in}\right) \\ &\approx r_i[n] - (1 - e^{j\Delta\phi_{in}}) r_i[n] - \frac{dr_i}{dt}(nT_s)\Delta\tau_{in} r_i[n] \end{aligned} \tag{16}$$

where $q(t) = \sum_{n=-\infty}^{\infty} \delta(t - (nT_s + \Delta\tau_{in}))$ and $(dr_i/dt)(nT_s)$ is the derivative of $r_i(t)$ at nT_s. The main impact of the phase noise and sampling jitter is the addition of an effective noise that will set a limit on the achievable SINR.

If the phase noise and sampling jitter sequences were known, their effects could be perfectly canceled. In practice, it is only possible to estimate this sequence with a tracking bandwidth $1/T_{est}$; this can be accomplished by embedding pilots in the data sequence[4] and is well studied in the phase noise literature [51]–[54]. This produces a low-bandwidth approximation of the effective noise. By subtracting out this noise estimate, the variance of the noise can be reduced, improving the SINR. In the limit of $T_{est} = T_s$ (ignoring practical difficulties of doing so), the entire effective noise sequence is estimated and can be canceled.

If the effective noise is uncorrelated at each element, it will be averaged by the beamforming summation [55]–[57]. However, because the effective noise is correlated with the signal, there is also a signal energy loss due to partially out-of-phase summation [55], [57]. This can be reduced by estimating the effective noise sequence, suggesting that each element should be equipped with a pilot tracking loop of bandwidth $1/T_{est}$, where T_{est} is chosen based on practically achievable estimation performance and system requirements. In [55], it was shown (for the case of only phase noise, but the result extends naturally with the inclusion of sampling jitter) that if the phase noise across elements is correlated below a bandwidth of approximately $1/T_{est}$, this pilot estimation loop can be performed at the array level rather than on a

[4]Embedding pilots comes at the cost of reducing the useful data rate. An alternative technique is to use decision-directed tracking, where hard decisions about constellation points are compared to the analog voltage to estimate the instantaneous phase rotation.

per-element basis. In this case, because the pilot estimation is performed after beamforming, it benefits from the array SINR gain of M, improving the estimation accuracy. At the same time, as long as the correlation bandwidth is no larger than $1/T_{\text{est}}$, there is no loss in the averaging gain for noise outside of this bandwidth. This level of correlation can be achieved by designing the PLL bandwidth at each element to be close to $1/T_{\text{est}}$. With this choice, below $1/T_{\text{est}}$ the phase noise and sampling jitter at each element track that of the common reference and are correlated across the entire array.

4) Summary: In summary, frequency synchronization in a massive array can be guaranteed by distributing a common reference to all transceivers and using a global carrier and sampling frequency recovery loop. Additionally, the effects of static LO and sampling clock skew are automatically calibrated by the beamforming algorithm. Finally, phase noise and sampling jitter can be averaged across the array to yield an array-level performance that is superior to any individual transceiver. This averaging can be managed by optimizing the PLL bandwidths at each element and using an array-level pilot tracking loop.

V. MM-WAVE ARRAYS

A. mm-Wave Signal Propagation

There is considerable interest in using the 60-GHz band for short-range wireless networks for video and high-speed data. Several standards exist for wireless HD video transmission (Wireless HD) and data (WiGig, 802.11ad) with rates approaching 10 G.

A common misconception is that signal propagation at mm-wave is worse than at lower frequencies. From the Friis equation, one would conclude that propagation loss is 100× worse at 60 GHz than at 6 GHz. However, conservation of energy indicates that in absence of absorbing media, the energy density of an isotropically transmitted waveform is the same at a given distance from the source regardless of the frequency. Naively applying the Friis equation will assume that the antenna gain is the same at 60 and 6 GHz. However, for the same antenna aperture, the gain of a 60-GHz antenna is larger than 6-GHz antenna by exactly the same factor, which means the energy received for a fixed aperture is identical. As a result, a more appropriate way to interpret the Friis equation is to say that the antenna size is constrained by the device form factor, which in turn sets the antenna gain.

What about absorption by the air? It is well known that the 60-GHz band is the "Oxygen Absorption Band" where the atmosphere is not the usually assumed lossless medium. However, to get a sense of this loss, take into account that even at the peak absorption frequency, the loss is below 10 dB/km in normal conditions.[5] These losses are substantial for a very long-range link, but for a distance <1 km, the extra losses can be easily absorbed into the link budget. Furthermore, transmission windows near 35 and 94 GHz do not suffer from significant atmospheric absorption [58].

One big difference between an RF and a mm-wave antenna is that for a fixed aperture, the mm-wave antenna has much higher directivity because it is large compared to the wavelength. High gain means that the mm-wave antenna is also highly directional, which is both a desirable and undesirable property. High directivity means that the antenna must point in the right direction for proper operation. However, a directive antenna also makes the system more robust to multipath propagation and interference since the antenna spatially filters these unwanted signals. The directivity can be harnessed by a phased array, in which the large aperture is composed of an array of antennas, electronically steerable by controlling the phase (and possibly amplitude) of each element.

When signals bounce off of walls or windows, it has been found that reflections are more specular at mm-wave frequencies. Also, materials tend to absorb more energy, so after a few reflections, the mm-wave signal dies off. This means that the best way to communicate in mm-wave bands is along a direct LOS, or perhaps after a few reflections. In contrast, at lower frequencies diffraction makes signal reflections more diffuse, creating many paths from source to destination, which leads to a complex time-varying channel best modeled in a statistical manner. As a result of these propagation characteristics, the possibility of doubling the data rate by polarization multiplexing is opened up at mm-wave. While reflections tend to mix the polarization [59], [60], mm-wave signals that propagate via LOS or with a limited number of reflections typically maintain enough polarization diversity to allow separation at the receiver. Under these conditions, it should be possible to equalize the cross-polarization contamination at the receiver. It is still unclear whether polarization multiplexing can be exploited in strongly non-LOS channels with many reflections.

For a fixed aperture, mm-wave and RF signal propagation have comparable propagation loss. However, because of antenna directivity, mm-wave links are more suited to point-to-point applications or environments with only a few reflections. Otherwise, there is no fundamental disadvantage to moving to a higher carrier frequency.[6] In fact, quite the opposite is true, as moving to higher frequency avails us of more bandwidth for communication, more secure channels (through use of directivity), and also

[5]Rain is an important loss mechanism that needs to be taken into account in the mm-wave link budget, adding an additional 10–30 dB of loss depending on the path length and frequency.

[6]Obviously, there are practical challenges to mm-wave implementations, such as lower aperture efficiency and difficulties designing efficient power amplifiers or low-noise amplifiers. However, these are engineering challenges rather than fundamental physical limits.

TABLE 1 Link Budget for a mm-Wave Downlink (Base Station to Mobile) and Uplink (Mobile to Base Station)

Link Budget Analysis	Downlink		Uplink	
Distance (km)	0.25	0.50	0.25	0.50
Transmiter power (dBm)	40	40	23	23
Transmit antenna gain (dBi)	25	25	12	12
Carrier frequency (GHz)	30	30	60	60
Free space prop. Loss (dB)	-110	-116	-116	-122
Other losses (shadowing, fading)	20	20	20	20
Receive antenna gain (dB)	12	12	35	35
Received power (dBm)	-53	-59	-66	-72
Bandwidth (GHz)	0.5	0.5	0.5	0.5
Thermal noise PSD (dBm/Hz)	-174	-174	-174	-174
Noise figure	7	7	5	5
Thermal noise (dBm)	-80	-80	-82	-82
SNR (dB)	27	21	16	10
Implementation loss	3	3	3	3
Shannon spectral eff.	8.0	6.0	4.4	2.6
Data rate (Gbps)	**4.0**	**3.0**	**2.2**	**1.3**

more degrees of freedom to share bandwidth through spatial diversity (in addition to time, frequency, and code).

1) mm-Wave Link Budget: The link budget for an exemplary mm-wave system is shown in Table 1 [3]. The downlink (base station to mobile) is at 30 GHz, the uplink at 60 GHz, and in both cases, the signal bandwidth is 500 MHz. Ranges of 0.25 and 0.5 km are considered. Achievable downlink data rates in excess of 4 Gb/s are possible with sufficient antenna gain. The Tx power and gain of the base station are fairly high at 40 dBm and 25 dBi, respectively, but in practice this can be efficiently realized with a large array of low-power transmitters. At the mobile, the required power and gain are more modest (23 dBm, 12 dBi) since mobile devices are smaller in size, have smaller energy sources, and their antennas are much more likely oriented in unfavorable direction. Based on today's CMOS technology, 39 dBm EIRP has been demonstrated using phased arrays [61] in the 60-GHz band, and it is not unreasonable to assume that similar levels can be achieved up to E-band.

2) mm-wave Link Budget Challenges: The link budget in Section V-A1 considered a LOS link. Non-LOS channels present a much more varied picture. Outdoor measurements across the mm-wave bands have found a fairly large difference in propagation loss exponent between LOS and NLOS paths; while LOS propagation is nearly free-space, NLOS paths can be severely affected by the reflection loss and increased path length [62]–[65]. The most benign NLOS environments are not much worse than LOS ones, but in the worst case, the capacity is significantly degraded. In indoor channels, it is found that NLOS paths at 60 GHz usually experience a path loss around 10 dB greater than LOS [66]. In summary, indoor or short-range NLOS links can be used quite reliably as long as there is sufficient link budget margin. Medium-range links can probably be set up in NLOS conditions with reasonable reliability, while long-range mm-wave communications may have to rely on LOS propagation. Finally, attenuation of signals through windows and walls is potentially higher at mm-wave frequencies, requiring higher margins in the link budget due to the variability of this loss as a function of construction materials.[7]

The problem of low-SNR network management is even more severe at mm-wave than RF since the array gain is more critical to achieving the desired link budget. Efficient protocols for user detection and registration and beamforming weight estimation are an active area of research. A related problem is user mobility; due to the smaller wavelength and narrower beams at mm-wave, tracking moving users is more challenging than at RF. It is currently unknown what user speeds can be supported with practical mm-wave systems.

B. Digital Versus Analog Beamforming

There is an important distinction between an MIMO receiver, where each antenna element has an independent ADC (Fig. 10), and a traditional phased array, with an RF phase shifter at each element (Fig. 11). Clearly, the MIMO digital architecture has a larger hardware footprint, but allows the greatest signal processing flexibility, including SU-MIMO, MU-MIMO, and phased array beamforming. An analog implementation, in contrast, can create an arbitrary antenna pattern (with gain and phase control at each element) for a single stream, but requires duplication of the full hardware to support multiple beams.

Another point to consider is the interference rejection provided by the two architectures. The dyanmic range of a wireless receiver is almost always limited by interferers rather than the signal of interest (the so-called "near–far problem"). By providing spatial filtering in the analog domain, analog beamforming is able to relax the linearity

[7]Since a significant fraction of mobile communication occurs indoors but most base stations are outdoors, it is very important to address this loss component.

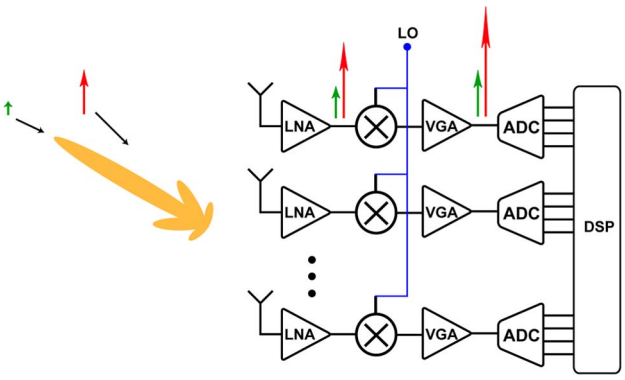

Fig. 10. *Fully digital MIMO system. Note that spatial filtering does not occur until the baseband, which means the entire front end is subject to interference from all directions.*

requirements of the receive chain by attenuating out-of-beam interferers. In contrast, since spatial filtering does not occur until after digitization, each receiver in the digital beamforming architecture must handle the full interferer strength.

1) Baseband Analog Beamforming and Nulling: Given that RF phase shifters are bulky and lossy, we have proposed baseband analog beamforming and nulling [67], which is accomplished by simply taking weighted combinations of the baseband I and Q waveforms. Current-domain summation can be implemented with minimal loss compared to RF combining, and the architecture is well suited to forming beams across the boundary of multiple chips, as high bandwidth currents can be routed off-chip and summed in an efficient manner.

On the transmitter side, baseband analog beamforming and nulling is even more compelling, as the phase shifting and amplitude scaling can be embedded into the analog modulation process with little overhead. In fact, due to the plethora of antennas, we can go one step further and use the array to not only do beamforming or nulling, but to form higher order constellations. In [68], we synthesized a 16-QAM waveform from an array of 4 I and 4 Q antenna elements. The antenna elements were partitioned akin to a segmented DAC, with three of the four elements unary weighted and a single-element binary weighted with 2-bits of resolution. This allowed the transmitters to be much more efficient by utilizing highly nonlinear switching amplifier topologies (Class E/F_2).

2) Hybrid Beamforming: An appealing architecture for mm-wave bands is a hybrid digital/analog approach where subarrays of antennas are controlled using analog beamforming. These subarrays can be used directly to sectorize the environment (Fig. 12) or can be followed by a lower-dimensional digital beamformer that is able to generate more complex beampatterns [69]–[72]. A hybrid architecture can balance the reduced complexity of analog beamforming with the greater flexibility of digital beamforming.

3) Interference Mitigation and Spatial Diversity: As we have seen, arrays of radios are used to minimize interference through transmit and receive beamforming, essentially filtering the signal in the angular domain. The detrimental impact of multipath propagation is also minimized since multipath components at most angles of arrival will be filtered by the receiver beampattern. Moreover, when a receiver link margin is not noise-limited, but rather interference-limited, some gain can be traded off and a beam null can be intentionally inserted into the pattern in the direction of an interferer (Fig. 13), in theory completely eliminating the undesired signal. In

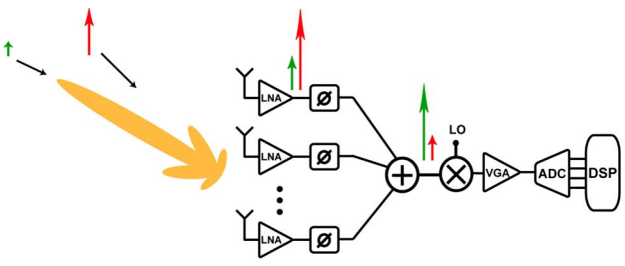

Fig. 11. *RF phase-shifting array. Since spatial filtering occurs at the front end after the phase shifters, the subsequent blocks have relaxed linearity requirements.*

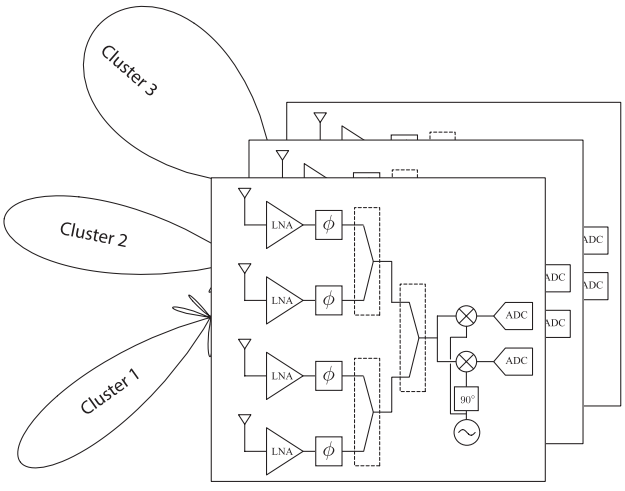

Fig. 12. *Hybrid analog/digital array receiver array. Note that a cluster of streams is routed to a subarray of antennas, each cluster pointing in a programmable direction through analog beamforming. Digital pattern shown is for illustrative purposes only; in reality, a generalized beam will be formed.*

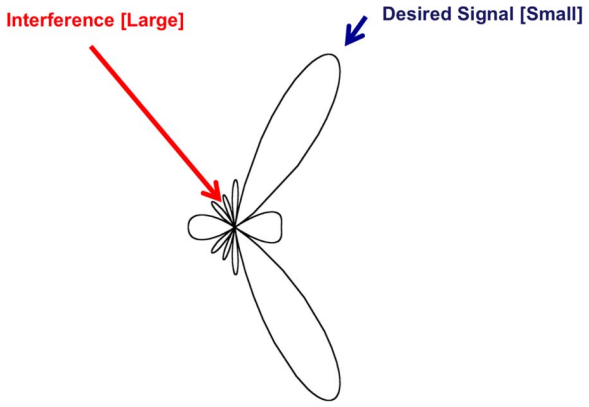

Fig. 13. ***Receiver that performs beamforming and nulling to maximize SNDR.***

practice, beam nulling requires very high precision in the beam coefficients, and any amplitude error (σ_ϵ) or phase mismatches (σ_δ), arising from quantization noise, phase noise, and other nonidealities, limits the peak-to-null ratio to $10\log(\sigma_\epsilon^2+\sigma_\delta^2)-10\log(M)$ [73].

4) True Time Delay Array: As discussed in Section III-A, when the propagation time across the array aperture is comparable to the symbol period, wideband beamforming techniques must be used. In a mm-wave system, this will almost always involve the use of analog TTD elements, which is generally bulkier and lossier than a phase shifter. In many cases, switched transmission lines, or artificial delay lines, are employed. In [74], an integrated variable time-delay architecture is proposed, but fundamentally the size of the realizable array is limited by the achievable maximum delay. The time-delay element can be embedded into the amplifiers in a chain, thereby absorbing device capacitance into the structure as well [75].

C. mm-Wave LO Distribution

Synchronization specifications for a large array are presented in Section IV-C, leading to an architecture where a common low-frequency reference is distributed across the array, and the LO and sampling clocks are generated locally for a single element or a small group of elements. One can think of this as taking a single PLL, segmenting it, and placing the segments close to antennas they serve. Since the phase noise of an oscillator is inversely proportional to its power dissipation, by exploiting the phase noise averaging, different amounts of PLL segmentation will, to first order, consume the same total power for a given system phase noise specification. However, due to factors such as PLL overhead power, routing loss, and VCO efficiency, the amount of segmentation will greatly affect the overall system power. The following sections will discuss these tradeoffs and how they influence the overall LO distribution architecture.

1) LO Routing: When planning the routing of a large array, one important consideration is the phase/delay shifting capability required of each element. Since even phased arrays can naturally calibrate for LO routing skew (Section IV-C2), signal distribution to a large number of elements will not necessarily require skew matching schemes such as H-trees. Therefore, the total route length can in principle grow linearly instead of exponentially.

Another important consideration is the ratio between LO power consumption required to meet the phase noise specification and the LO power that needs to be delivered to the load. If these are similar, then any routing losses will dissipate significant amounts of power. If instead the load requires much higher power levels than the source, the LO can be routed with little efficiency loss and gain elements can be used at the load to deliver the required power. In practice, due to the limited achievable transmission line impedances, it will be necessary to distribute gain elements along the LO distribution network. This reduces the efficiency, but allows for more realistic line impedances.

2) VCO Efficiency: As mentioned earlier, the phase noise of an oscillator is inversely proportional to the power dissipated. The VCO figure of merit (FOM) is a useful metric to compare multiple VCOs at different phase noise levels

$$FOM = 10\log\left(\frac{\mathcal{L}\{\Delta f\}\left(\frac{P_{\mathrm{DC}}}{1\ \mathrm{mW}}\right)^2}{\left(\frac{f_0}{\Delta f}\right)}\right). \tag{17}$$

Here, $\mathcal{L}\{\Delta f\}$ is the phase noise at offset frequency Δf from the resonance frequency f_0, and P_{DC} is the oscillator's power consumption. It has been discussed in [76] that for any LC oscillator with efficiency η, noise factor F, and tank quality factor Q, the FOM can be described in the following form:

$$FOM = 10\log\left(\frac{kTF}{2\eta Q^2}10^{-3}\right) \tag{18}$$

and that for an efficiency of 100% and a noise factor of $(1+\gamma)$, the maximum achievable FOM is

$$FOM_{\mathrm{opt}} = -174.6 - 20\log Q. \tag{19}$$

In [76], a VCO within 1.5 dB of this optimal FOM was demonstrated at RF. While efficiencies will typically be

lower at mm-wave, for a given VCO topology, the FOM is largely dependent on the tank Q.

When the system's PLL is divided into N_{PLL} segments, the power of each VCO should decrease by N_{PLL}, and its noise should increase by the same factor for constant FOM. However, to reduce the power, the tank impedance will also need to be increased by N_{PLL}. Achievable values of Q may vary dramatically for different tank impedances, which will change the FOM and cause the power–noise tradeoff to deviate from the ideal relationship. For instance, very large values of inductance may lead to operation too close to the self-resonant frequency (SRF), and very small values of inductance may require small wires and be highly resistive. When deciding on the level of PLL segmentation, the achievable tank impedances will affect the range of feasible options and may significantly change the optimum. At mm-wave frequencies, even relatively small inductances will yield large tank impedances with good Q, which may drive mm-wave systems to higher levels of optimum segmentation than RF systems.

3) PLL Bandwidth: In most situations, a low-frequency crystal reference will be required to achieve the specified frequency error and low-frequency phase noise. The available frequencies of crystals range from the low-MHz range up to a few hundred MHz, with a phase noise floor on the order of −150 dBc/Hz. In RF systems, frequency multiplication will lead to in band reference noise on the order of −115 dBc/Hz, which is well within tolerable levels for high-order constellations, even with relatively low carrier recovery (CR) bandwidths. At mm-wave, since the reference frequency is multiplied by around 1000×, the in-band phase noise of the PLL is limited to approximately −90 dBc/Hz. This will potentially be a significant contributor to the overall integrated phase error and limit the constellation order, unless aggressive CR bandwidths are pursued.

Traditionally, for a given reference noise and oscillator noise level, the PLL bandwidth is selected to achieve the lowest amount of integrated phase noise at the PLL output. In Section IV-C3, it was shown that the PLL bandwidth should be set close to the CR bandwidth. Combining these two requirements, the optimum value of the PLL bandwidth will be a function of both the CR bandwidth and the relative noise levels between the reference and oscillator as in a conventional PLL design. The choice of the common reference frequency will also depend upon the CR bandwidth and the optimal PLL bandwidth.

D. Antennas and Packaging Challenges at mm-Wave

Two key challenges in realizing a complete mm-wave phased array system are the IC packaging and antenna design. Leveraging advanced printed circuit board (PCB) fabrication techniques, high-performance RF substrates, and high-density flip-chip packaging is critical to meet these challenges.

1) Overview: Unlike at lower frequencies, where antennas and packaging may be decoupled in practice, at mm-wave they are typically co-optimized to minimize routing losses and control parasitic coupling. The result is a combined chip-antenna module, with only low-frequency electrical interfaces to the outside world, other than the transmitted and received electromagnetic radiation from the antennas themselves. Modules are typically realized as a ball-grid array (BGA) package built on a low-loss substrate, such as low-temperature co-fired ceramic (LTCC) or high-performance laminates such as Rogers 4003C [77] or Taconic TLY-05 [78]. An example diagram of a mm-wave BGA module previously characterized at the BWRC is shown in Fig. 14.

The inductances and capacitances associated with conventional bondwire-based packaging become increasingly problematic at mm-wave frequencies, which lead to the use of flip-chip packaging techniques. Since flip-chip also allows for area-array IO pads (in the interior of the chip, as well as around the perimeter), it also helps to reduce routing complexity in phased arrays with many elements. Antenna elements can be directly above the corresponding transceiver element on the RFIC without having to increase element-to-element spacing, or resorting to convoluted phase-matched routing lines.

BGA packages also tend to have many metallization layers, each satisfying different requirements. RF feedlines and antennas can be on their own layers to minimize coupling to the rest of the circuits. Thicker power planes on separate layers minimize ohmic losses in the supply networks. IF outputs and digital control signals may be on yet another routing layer. The result is a complex, multilayer stack that can have as little as 4 or as many as 12 or more routing layers [79], [80]. Dielectric materials and thicknesses must be carefully chosen to optimize antenna performance.

2) Antenna Design: For the base station, particularly in a sectorized system, higher-gain antennas such as horn arrays can be employed to increase gain while trading off beam-steering range. In mobile devices, the vast majority of mm-wave antenna modules make use of microstrip patch antennas, which is compatibile with planar PCB and

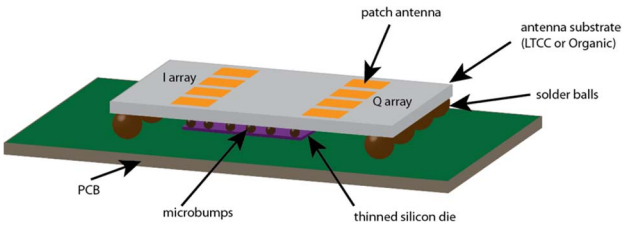

Fig. 14. *mm-wave antenna module with BGA footprint, implementing a quadrature spatial combining transmitter [68], [79]. To reduce its impact on the radiation pattern, the silicon RFIC is attached on the opposite side of the package as the antennas.*

packaging technologies. Additionally, the ground plane of the patch helps isolate signals on lower layers from the antenna and feedlines. Patch antennas are typically fairly narrowband unless implemented on thick and/or low dielectric constant substrates [81]. Substrates cannot be made arbitrarily thick without losses from surface waves, so to further increase bandwidth, aperture, or proximity, coupling is used [82].

To reduce unwanted radiation and coupling from antenna feedlines, RF routing layers have a completely opposite set of criteria from the substrate. Thin, high dielectric constant layers are desirable in this case. This mismatch in substrate requirements is one of the factors leading to increased package complexity, as separate RF routing and antenna layers are needed.

3) Large-Scale Array Integration: Developing a large-scale phased array that integrates many die or modules presents additional challenges. To avoid grating lobes in the radiation pattern, antenna elements should be spaced at $\lambda/2$. This requires adjacent modules to be closely abutted, creating additional problems in routing signals from the BGA pads. Conversely, including many die in a single package increases the area and routing complexity of the package, driving up its cost. Some success has been demonstrated in scalable array archictures using conventional BGA techniques but with an aggressive layer count [80] or more experimental wafer-level packaging [83].

VI. CONCLUSION

In this paper we have reviewed the state of the art in large antenna arrays for massive MIMO and presented key algorithms, architectures, and design techniques to build these systems in a cost- and energy-efficient manner at both RF and mm-wave frequencies. Arrays and their associated spatial signal processing techniques are a key technology for interference mitigation at both the base station as well as certain user devices. Cost- and energy-efficient arrays are therefore a central element in our vision of an xG network where a wide range of devices—from energy-starved sensors to high-power personal computers—communicate with the network over directional, high-bandwidth links even in very dense environments. Additionally, deploying very highly directional xG hubs in a wireless mesh network can significantly speed up and lower the cost of network infrastructure deployment while making the network itself more robust. Though there are many open research questions in both implementation and network management, large arrays look to be a very promising technology. ■

Acknowledgment

Special thanks to the DARPA TEAM program (60 GHz), the DARPA Wafer Scale Radio Seedling [84], the FCRP-C2S2 Program, and continuing programs such as the NSF THz Chip-to-Chip (ECCS-1201755), NSF EARS, and the DARPA RF-FPGA and Arrays at Commercial Timescale (ACT) programs.

REFERENCES

[1] A. M. Niknejad *et al.*, "The xG Vision: Making the Internet truly wireless." [Online]. Available: http://files-eu.clickdimensions.com/ericssoncom-anlg4/documents/xg_vision_5g_public_.pdf

[2] ITU "Framework and overall objectives of the future development of IMT for 2020 and beyond," presented at the 18th Meeting of ITU Working Party 5D, Feb. 2014.

[3] C. J. Zhang, "Realizing massive MIMO in LTE-Advanced and 5G," presented at the Brooklyn 5G Summit, Apr. 2015.

[4] B. V. Veen and K. Buckley, "Beamforming: A versatile approach to spatial filtering," *IEEE ASSP Mag.*, vol. 5, no. 2, pp. 4–24, Apr. 1988.

[5] Increasing capacity in wireless broadcast systems using Distributed Transmission/Directional Reception (DTDR), by A. J. Paulraj and T. Kailath, U.S. 1994, Patent 5 345 599. [Online]. Available: http://www.google.com/patents/US5345599

[6] S. Talwar, M. Viberg, and A. J. Paulraj, "Blind estimation of multiple co-channel digital signals using an antenna array," *IEEE Signal Process. Lett.*, vol. 1, no. 2, pp. 29–31, Feb. 1994.

[7] G. J. Foschini and M. J. Gans., "On limits of wireless communications in a fading environment when using multiple antennas," *Wireless Pers. Commun.*, vol. 6, pp. 311–335, Mar. 1998.

[8] I. E. Telatar, "Capacity of multi-antenna Gaussian channels," *Eur. Trans. Telecommun.*, vol. 10, no. 6, pp. 585–595, 1999.

[9] P. Wolniansky, G. J. Foschini, G. D. Golden, and R. Valenzuela, "V-BLAST: An architecture for realizing very high data rates over the rich-scattering wireless channel," in *Proc. URSI Int. Symp. Signals, Syst. Electron.*, 1998, pp. 295–300.

[10] Wireless LAN Media Access Control (MAC) and Physical Layer (PHY) Specifications, IEEE Std. 802.11n-2009, 2009.

[11] Evolved Universal Terrestrial Radio Access (E-UTRA); LTE Physical Layer; General Description, 3GPP Std. TS 36.201, 2015.

[12] TDM-based fixed wireless loop system, by D. Avidor, S. Kasturia, T. Sizer, R. Valenzuela, and G. A. Wright, U.S. Patent 6 961 325, 2005. [Online]. Available: http://www.google.com/patents/US6961325

[13] Evolved Universal Terrestrial Radio Access (E-UTRA); LTE Physical Layer; General Description, 3GPP Std. TS 36.201 V8.3.0, Mar. 2009.

[14] T. L. Marzetta, "Noncooperative cellular wireless with unlimited numbers of base station antennas," *IEEE Trans. Wireless Commun.*, vol. 9, no. 11, pp. 3590–3600, Nov. 2010.

[15] X. Gao, F. Tufvesson, O. Edfors, and F. Rusek, "Measured propagation characteristics for very-large MIMO at 2.6 GHz," in *Conf. Rec. 46th Asilomar Conf. Signals, Syst. Comput.*, Nov. 2012, pp. 295–299.

[16] J. Hoydis, S. ten Brink, and M. Debbah, "Comparison of linear precoding schemes for downlink massive MIMO," in *Proc. IEE ICC*, Jun. 2012, pp. 2135–2139.

[17] J. Hoydis, S. ten Brink, and M. Debbah, "Massive MIMO in the UL/DL of cellular networks: How many antennas do we need?" IEEE J. Sel. Areas Commun., vol. 31, no. 2, pp. 160–171, Feb. 2013.

[18] Z. Pi and F. Khan, "A millimeter-wave massive MIMO system for next generation mobile broadband," in *Conf. Rec. 46th Asilomar Conf. Signals, Syst. Comput.*, Nov. 2012, pp. 693–698.

[19] T. S. Rappaport *et al.*, "Millimeter wave mobile communications for 5G cellular: It will work!" IEEE Access, vol. 1, pp. 335–349, 2013.

[20] GreenTouch, (2011), GreenTouch Consortium. [Online]. Available: http://www.greentouch.org/index.php?page=members-collaborate-on-dramatic-new-antenna-system

[21] H. Suzuki *et al.*, "Highly spectrally efficient Ngara rural wireless broadband access demonstrator," in *Proc. Int. Symp. Commun. Inf. Technol. (ISCIT)*, Oct. 2012, pp. 914–919.

[22] H. Suzuki *et al.*, "Large-scale multiple antenna fixed wireless systems for rural areas," in *Proc. 23rd IEEE Int. Symp. Pers. Indoor Mobile Radio Commun. (PIMRC)*, Sep. 2012, pp. 1600–1605.

[23] X. Huang, Y. J. Guo, A. Zhang, and V. Dyadyuk, "A multi-gigabit microwave backhaul," *IEEE Commun. Mag.*, vol. 50, no. 3, pp. 122–129, Mar. 2012.

[24] H. V. Balan *et al.*, "USC SDR, an easy-to-program, high data rate, real time software radio platform," in *Proc. ACM SIGCOMM 2nd*

Workshop Softw. Radio Implement. Forum, Aug. 2013, pp. 25–30.

[25] C. Shepard *et al.*, "Argos: Practical many-antenna base stations," in *Proc. 18th Int. Conf. Mobile Comput. Netw. (MobiCom)*, Aug. 2012, pp. 53–64.

[26] C. Shepard, H. Yu, and L. Zhong, "ArgosV2: A flexible many-antenna research platform," in *Proc. 19th Int. Conf. Mobile Comput. Netw. (MobiCom)*, Oct. 2013, pp. 163–166.

[27] H. Yang and T. L. Marzetta, "Performance of conjugate and zero-forcing beamforming in large-scale antenna systems," *IEEE J. Sel. Areas Commun.*, vol. 31, no. 2, pp. 172–179, Feb. 2013.

[28] J. Vieira *et al.*, "A flexible 100-antenna testbed for massive MIMO," in *Proc. IEEE GLOBECOM 2014 Workshops*, Dec. 2014, pp. 287–293.

[29] X. Gao, O. Edfors, F. Rusek, and F. Tufvesson, "Massive MIMO performance evaluation based on measured propagation data," *IEEE Trans. Wireless Commun.*, vol. 14, no. 7, pp. 3899–3911, Jul. 2015.

[30] Mimosa Networks. [Online]. Available: http://www.mimosanetworks.com

[31] Ubiquiti Networks. [Online]. Available: http://www.ubnt.com

[32] E. Larsson, O. Edfors, F. Tufvesson, and T. L. Marzetta, "Massive MIMO for next generation wireless systems," *IEEE Commun. Mag.*, vol. 52, no. 2, pp. 186–195, Feb. 2014.

[33] H. Huh, G. Caire, H. C. Papadopoulos, and S. A. Ramprashad, "Achieving 'massive MIMO' spectral efficiency with a not-so-large number of antennas," *IEEE Trans. Wireless Commun.*, vol. 11, no. 9, pp. 3226–3239, Sep. 2012.

[34] Y. Kim *et al.*, "Evolution beyond LTE-advanced with full dimension MIMO," in *Proc. 2013 IEEE Int. Conf. Commun. (ICC) Workshops*, 2013, pp. 111–115.

[35] Y.-H. Nam *et al.*, "Full-dimension MIMO (FD-MIMO) for next generation cellular technology," *IEEE Commun. Mag.*, vol. 51, no. 6, pp. 172–179, Jun. 2013.

[36] Y. Kim *et al.*, "Full dimension MIMO (FD-MIMO): The next evolution of MIMO in LTE systems," *IEEE Wireless Commun. Mag.*, vol. 21, no. 2, pp. 92–100, Jun. 2014.

[37] B. Lee, J. Choi, J.-Y. Seol, D. J. Love, and B. Shim, "Antenna grouping based feedback reduction for FDD-based massive MIMO systems," in *Proc. IEEE Int. Conf. Commun. (ICC)*, Jun. 2014, pp. 4477–4482.

[38] Z. Jiang, A. F. Molisch, G. Caire, and Z. Niu, "Achievable rates of FDD massive MIMO systems with spatial channel correlation," *IEEE Trans. Wireless Commun.*, vol. 14, no. 5, pp. 2868–2882, May 2015.

[39] F. Rusek *et al.*, "Scaling up MIMO: Opportunities and challenges with very large arrays," *IEEE Signal Process. Mag.*, vol. 30, no. 1, pp. 40–60, Jan. 2013.

[40] L. Lu, G. Y. Li, A. L. Swindlehurst, A. Ashikhmin, and R. Zhang, "An overview of massive MIMO: Benefits and challenges," *IEEE J. Sel. Topics Signal Process.*, vol. 8, no. 5, pp. 742–758, Oct. 2014.

[41] H. Q. Ngo, E. G. Larsson, and T. L. Marzetta, "Massive MU-MIMO downlink TDD systems with linear precoding and downlink pilots," in *Proc. 51st Allerton Conf. Commun., Control, Comput.*, Oct. 2013, pp. 293–298.

[42] E. Luther, "5G massive MIMO testbed: From theory to reality," National Instruments, Tech. Rep. [Online]. Available: http://www.ni.com/white-paper/52382/en/

[43] M. Brown and M. Turgeon, "TitanMIMO: A 100×100 massive MIMO testbed based on xTCA," Nutaq Corp., Tech. Rep. [Online]. Available: http://www.nutaq.com

[44] A. Puglielli *et al.*, "A scalable massive MIMO array architecture based on common modules," in *Proc. 2015 IEEE Int. Conf. Commun. (ICC) Workshops*, Jun. 2015, pp. 1284–1289.

[45] L. Kong, "Energy-efficient 60 GHz phased-array design for multi-Gb/s communication systems," Ph.D. dissertation, EECS Department, University of California, Berkeley, CA, USA, Dec. 2014.

[46] H. Q. Ngo, E. G. Larsson, and T. L. Marzetta, "Energy and spectral efficiency of very large multiuser MIMO systems," *IEEE Trans. Commun.*, vol. 61, no. 4, pp. 1436–1449, Apr. 2013.

[47] K. F. Warnick, M. Ivashina, R. Maaskant, and B. Woestenburg, "Unified definitions of efficiencies and system noise temperature for receiving antenna arrays," *IEEE Trans. Antennas Propag.*, vol. 58, no. 3, pp. 2121–2125, Mar. 2010.

[48] K. F. Warnick and B. Jeffs, "Efficiencies and system temperature for a beamforming array," *IEEE Antennas Wireless Propag. Lett.*, vol. 7, pp. 565–568, 2008.

[49] M. Ivashina, R. Maaskant, and B. Woestenburg, "Equivalent system representation to model the beam sensitivity of receiving antenna arrays," *IEEE Antennas Wireless Propag. Lett.*, vol. 7, pp. 733–737, 2008.

[50] K. Lauritzen, "Correlation of signals, noise, harmonics in parallel analog-to-digital converter arrays," Ph.D. dissertation, ECE Department, University of Maryland, College Park, MD, USA, Dec. 2009. [Online]. Available: http://hdl.handle.net/1903/9608

[51] S. Wu and Y. Bar-Ness, "OFDM systems in the presence of phase noise: Consequences and solutions," *IEEE Trans. Commun.*, vol. 52, no. 11, pp. 1988–1996, Nov. 2004.

[52] S. Wu and Y. Bar-Ness, "A phase noise suppression algorithm for OFDM-based WLANs," *IEEE Commun. Lett.*, vol. 6, no. 12, pp. 535–537, Dec. 2002.

[53] P. Robertson and S. Kaiser, "Analysis of the effects of phase noise in orthogonal frequency division multiplex (OFDM) systems," in *Proc. IEEE Int. Conf. Commun. (ICC)*, Jun. 1995, pp. 1652–1657.

[54] D. Petrovic, W. Rave, and G. Fettweis, "Effects of phase noise on OFDM systems with and without PLL: Characterization and compensation," *IEEE Trans. Commun.*, vol. 55, no. 8, pp. 1607–1616, Aug. 2007.

[55] A. Puglielli *et al.*, "Phase Noise Scaling and Tracking in OFDM Multi-user Beamforming Arrays," in review.

[56] T. Höhne and V. Ranki, "Phase noise in beamforming," *IEEE Trans. Wireless Commun.*, vol. 9, no. 12, pp. 3682–3689, Dec. 2010.

[57] A. Pitarokoilis, S. K. Mohammed, and E. G. Larsson, "Uplink performance of time-reversal MRC in massive MIMO systems subject to phase noise," *IEEE Trans. Wireless Commun.*, vol. 14, no. 2, pp. 711–723, Feb. 2015.

[58] Federal Communications Commission, Office of Engineering and Technology, New Technology Development DivisionMillimeter wave propagation: Spectrum management implications, Tech. Rep. Bulletin Number 70, Jul. 1997.

[59] C. Waldschmitt, C. Kuhnert, S. Schulteis, and W. Wiesbeck, "Compact MIMO-arrays based on polarisation-diversity," in *Proc. IEEE Int. Symp. Antennas Propag.*, Jun. 2003, pp. 499–502.

[60] R. Salman, I. Willms, L. Reichardt, T. Zwick, and W. Wiesbeck, "On polarization diversity gain in short range UWB-radar object imaging," in *Proc. IEEE Int. Conf. Ultra-Wideband (ICUWB)*, Sep. 2012, pp. 402–406.

[61] A. Valdes-Garcia *et al.*, "Single-element and phased-array transceiver chipsets for 60 GHz Gb/s communications," *IEEE Commun. Mag.*, vol. 49, no. 4, pp. 120–131, Apr. 2011.

[62] N. Shuai, G. R. MacCartney, S. Shu, and T. S. Rappaport, "72 GHz millimeter wave indoor measurements for wireless and backhaul communications," in *Proc. 24th IEEE Int. Symp. Pers. Indoor Mobile Radio Commun. (PIMRC)*, Sep. 2013, pp. 2429–2433.

[63] M. Samimi *et al.*, "28 GHz angle of arrival and angle of departure analysis for outdoor cellular communications using steerable beam antennas in New York City," in *Proc. 77th IEEE Veh. Technol. Conf. (VTC Spring)*, Jun. 2013, pp. 1–6.

[64] T. S. Rappaport *et al.*, "Broadband millimeter-wave propagation measurements and models using adaptive-beam antennas for outdoor urban cellular communications," *IEEE Trans. Antennas Propag.*, vol. 61, no. 4, pp. 1850–1859, Apr. 2012.

[65] S. Rangan, T. S. Rappaport, and E. Erkip, "Millimeter-wave cellular wireless networks: Potentials and challenges," *Proc. IEEE*, vol. 102, no. 3, pp. 366–385, Mar. 2014.

[66] X. Hao, V. Kukshya, and T. Rappaport, "Spatial and temporal characteristics of 60 GHz indoor channels," *IEEE J. Sel. Areas Commun.*, vol. 20, no. 3, pp. 620–630, Apr. 2002.

[67] M. Tabesh *et al.*, "A 65 nm CMOS 4-element sub-34 mW/element 60 GHz phased-array transceiver," *IEEE J. Solid-State Circuits*, vol. 46, no. 12, pp. 3018–3032, Dec. 2011.

[68] J. Chen *et al.*, "A digitally modulated mm-wave cartesian beamforming transmitter with quadrature spatial combining," in *Int. Solid-State Circuits Conf. (ISCC) Dig. Tech. Papers*, Feb. 2013, pp. 232–233.

[69] A. Alkhateeb, O. E. Ayach, G. Leus, and R. W. Heath, "Channel estimation and hybrid precoding for millimeter wave cellular systems," *IEEE J. Sel. Topics Signal Process.*, vol. 8, no. 5, pp. 831–846, Oct. 2014.

[70] A. Alkhateeb, J. Mo, N. G. Prelcic, and R. W. Heath, "MIMO precoding and combining solutions for millimeter-wave systems," *IEEE Commun. Mag.*, vol. 52, no. 12, pp. 122–131, Dec. 2014.

[71] W. Roh *et al.*, "Millimeter-wave beamforming as an enabling technology for 5G cellular communications: Theoretical feasibility and prototype results," *IEEE Commun. Mag.*, vol. 52, no. 2, pp. 106–113, Feb. 2014.

[72] O. E. Ayach, S. Rajagopal, S. Abu-Surra, Z. Pi, and R. W. Heath, "Spatially sparse precoding in millimeter wave MIMO systems," *IEEE Trans. Wireless Commun.*, vol. 13, no. 3, pp. 1499–1513, Mar. 2014.

[73] O. Bakr, "A scalable and cost effective architecture for high gain beamforming antennas," U.C. Berkeley, Tech. Rep. No. UCB/EECS-2010-178, Dec. 2010.

[74] E. Adabi and A. M. Niknejad, "Broadband variable passive delay elements based on an inductance multiplication technique," in *Proc. IEEE Radio Freq. Integrated Circuits Symp.*, Jun. 2008, pp. 445–448.

[75] E. A. Firouzjaei, "mm-wave phase shifters and switches," Ph.D. dissertation, EECS

Department, University of California, Berkeley, CA, USA, Dec. 2010. [Online]. Available: http://www.eecs.berkeley.edu/Pubs/TechRpts/2010/EECS-2010-163.html

[76] T. L. Marzetta, "Noncooperative cellular wireless with unlimited numbers of base station antennas," *IEEE Trans. Wireless Commun.*, vol. 9, no. 11, pp. 1436–1449, Nov. 2010.

[77] Rogers Corporation, (2015), RO4000 series high frequency circuit materials. [Online]. Available: http://www.rogerscorp.com/documents/726/acs/RO4000-LaminatesDatasheet.pdf

[78] Taconic Advanced Dielectric Division, (2012), TLY family of low-loss laminates. [Online]. Available: http://www.taconic-add.com/pdf/tly.pdf

[79] D. Titz *et al.*, "Antenna-array topologies for mm-wave beamforming transmitter with quadrature spatial combining," in *Proc. IEEE-APS Top. Conf. Antennas Propag. Wireless Commun. (APWC)*, Aug. 2014, pp. 399–402.

[80] X. Gu *et al.*, "A compact 4-chip package with 64 embedded dual-polarization antennas for W band phased-array transceivers," in *Proc. 64th IEEE Electron. Compon. Technol. Conf. (ECTC)*, May 2014, pp. 1272–1277.

[81] R. Waterhouse, *Microstrip Patch Antennas: A Designer's Guide*. New York, NY, USA: Springer-Verlag, 2003.

[82] D. G. Kam, D. Liu, A. Natarajan, S. Reynolds, and B. Floyd, "Organic packages with embedded phased-array antennas for 60 GHz wireless chipsets," *IEEE Trans. Compon. Packag. Manuf. Technol.*, vol. 1, no. 11, pp. 1806–1814, Nov. 2011.

[83] W. Shin, B.-H. Ku, O. Inac, Y.-C. Ou, and G. Rebeiz, "A 108 GHz 4 × 4 wafer-scale phased array transmitter with high-efficiency on-chip antennas," *IEEE J. Solid-State Circuits*, vol. 48, no. 9, pp. 2041–2055, Sep. 2013.

[84] A. M. Niknejad, E. Alon, B. Nikolic, and J. Rabaey, "Wafer scale distributed radio," Air Force Research Laboratory, Tech. Rep. ARFL-RY-WP-TR-2009-1172. [Online]. Available: http://www.dtic.mil/cgi-bin/GetTRDoc?Location=U2&doc=GetTRDoc.pdf&AD=ADA504367

ABOUT THE AUTHORS

Antonio Puglielli (Student Member, IEEE) received the B.S. degree in applied math, engineering, and physics (AMEP) from the University of Wisconsin-Madison, Madison, WI, USA, in 2013, and is currently pursuing the Ph.D. degree in electrical engineering at the University of California, Berkeley, CA, USA.

He has held internship positions with National Instruments, Qualcomm, and Intel. His current research interests are in the field of analog and digital signal processing algorithms, circuits, and systems.

Andrew Townley (Student Member, IEEE) received the B.S. and M.S. degrees in electrical engineering from the University of Pennsylvania, Philadelphia, PA, USA, in 2011, and is currently pursuing the Ph.D. degree in electrical engineering at the University of California, Berkeley, CA, USA.

During his Ph.D. career, he has held internship positions with Nokia, Analog Devices, and Google. His current research interests are in millimeter-wave circuit design and packaging for sensing and communication applications.

Greg LaCaille (Student Member, IEEE) received the B.S. and M.S. degree in electrical engineering from California Polytechnic State University, San Luis Obispo, CA, USA, in 2010, and is currently pursuing the Ph.D. degree in electrical engineering at the University of California, Berkeley, CA, USA.

Between 2010 and 2012, he worked with the Lawrence Livermore National Laboratory, Livermore, CA, USA, designing X-ray diagnostics for experiments at the National Ignition Facility. He has interned with Altera, Apple, and Intel working on integrated circuit frequency synthesizers. He is an active member of the Berkeley Wireless Research Center (BWRC). His research interests are in energy-efficient frequency synthesizers, integrated circuit design for RF and millimeter-wave phased arrays, and design automation of analog/RF integrated circuits.

Vladimir Milovanović received the Dipl.-Ing. degree in electrical engineering from the University of Belgrade, Belgrade, Serbia, in 2005, and the Ph.D. degree from Delft University of Technology, Delft, The Netherlands, in 2010.

Since the beginning of 2014, he has been working as a Postdoctoral Scholar with the University of California, Berkeley, CA, USA, under the guidance of Prof. Borivoje Nikolić. During the studies, he was on internships with the Technion—Israel Institute of Technology, Haifa, Israel, in summer 2004 and the Technical University of Madrid, Madrid, Spain, in spring 2005. Before joining Berkeley's Department of Electrical Engineering and Computer Sciences, from 2011 he was with Vienna University of Technology, Vienna, Austria, as a Postdoctoral Research Fellow.

His research interests include design, modeling, and optimization of CMOS/BiCMOS analog, mixed-signal, and digital integrated circuits, devices, and systems, as well as development and implementation of energy-efficient communication, control, and signal processing algorithms.

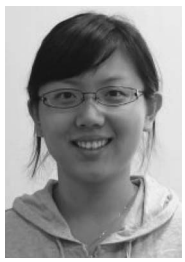

Pengpeng Lu received the Bachelor of Science degree from Peking University, Beijing, China, in 2012, and the M.S. degree from the University of California, Berkeley, CA, USA, in 2015, and is currently pursuing the Ph.D. degree in electrical engineering and computer science at the University of California, Berkeley.

From May to December 2014, she was an Intern with Marvell, Inc., Santa Clara, CA, USA, where she was involved with design and simulation of digitally controlled ring oscillators for wireless applications. Her research interests are mixed-signal circuits and design of energy-efficient RF front-end circuits.

Konstantin Trotskovsky received the B.S. and M.S. degrees in electrical engineering from the Technion—Israel Institute of Technology, Haifa, Israel, in 2004 and 2010, respectively, and is currently pursuing the Ph.D. degree at the University of California, Berkeley, CA, USA.

From 2004 to 2013, he was with the Israel Defense Forces (IDF) R&D unit, working on various analog and RF projects. His research focuses on RF receivers design for large antenna arrays.

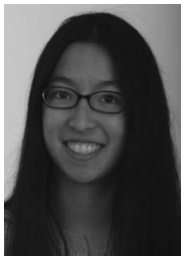

Amy Whitcombe received the B.S. degree in electrical and computer engineering from Olin College, Needham, MA, USA, in 2013, and is currently pursuing the Ph.D. degree in electrical engineering at the University of California, Berkeley, CA, USA.

Her research interests includedeeply scaled CMOS technology variability and analog-to-digital converters for energy-efficient wireless receivers.

Nathan Narevsky (Student Member, IEEE) received the B.S. degree in electrical engineering and computer science from the University of California, Berkeley, CA, USA, in 2012, and is currently pursuing the Ph.D. degree in electrical engineering at the Berkeley Wireless Research Center.

In 2012, he was an intern with Intel working on integrated voltage regulators for next-generation microprocessor dynamic voltage and frequency scaling. In 2015, he was an intern with Intel Labs working on mixed-signal equalizers for next-generation millimeter-wave communication systems. His research interests include energy-efficient analog and mixed-signal circuit and system design for various applications, including array radio systems and biomedical devices.

Gregory Wright received the bachelor's degree in physics from Harvard University, Cambridge, MA, USA, the M.A. degree in mathematics from Cambridge University, Cambridge, U.K., and the Ph.D. degree in physics from Princeton University, Princeton, NJ, USA.

He did his postdoctoral studies with Bell Labs in millimeter-wave astronomy and was a co-investigator on the Antarctic Submillimeter Telescope and Remote Observatory (AST/RO), the first permanent astronomical observatory at the South Pole. He was a Researcher with Bell Labs from 1994 until 2001, after which he co-founded startups in network performance measurement and RFID systems. He joined Alcatel-Lucent Bell Labs, Holmdel, NJ, USA, in 2010 as a member of wireless communication research, where he has worked on new approaches for energy-efficient radios.

Thomas Courtade (Member, IEEE) received the B.Sc. degree (*summa cum laude*) in electrical engineering from Michigan Technological University, Houghton, MI, USA, in 2007, and the M.S. and Ph.D. degrees from the University of California, Los Angeles (UCLA), CA, USA, in 2008 and 2012, respectively.

He is an Assistant Professor with the Department of Electrical Engineering and Computer Sciences, University of California, Berkeley, CA, USA. Prior to joining UC Berkeley in 2014, he was a Postdoctoral Fellow supported by the NSF Center for Science of Information.

Dr. Courtade's honors include a Distinguished Ph.D. Dissertation Award and an Excellence in Teaching Award from the UCLA Department of Electrical Engineering, and a Jack Keil Wolf Student Paper Award for the 2012 International Symposium on Information Theory.

Elad Alon received the B.S., M.S., and Ph.D. degrees in electrical engineering from Stanford University, Stanford, CA, USA, in 2001, 2002, and 2006, respectively. In 2007, he joined the University of California, Berkeley, CA, USA, where he is now an Associate Professor of electrical engineering and computer sciences as well as a co-director of the Berkeley Wireless Research Center (BWRC). He has held advisory, consulting, or visiting positions with Lion Semiconductor, Cadence, Xilinx, Wilocity, Oracle, Intel, AMD, Rambus, Hewlett Packard, and IBM Research, where he worked on digital, analog, and mixed-signal integrated circuits for computing, test and measurement, power management, and high-speed communications. His research focuses on energy-efficient integrated systems, including the circuit, device, communications, and optimization techniques used to design them.

Dr. Alon received the IBM Faculty Award in 2008, the 2009 Hellman Family Faculty Fund Award, as well as the 2010 UC Berkeley Electrical Engineering Outstanding Teaching Award, and has coauthored papers that received the 2010 ISSCC Jack Raper Award for Outstanding Technology Directions Paper, the 2011 Symposium on VLSI Circuits Best Student Paper Award, and the 2012 as well as the 2013 Custom Integrated Circuits Conference Best Student Paper Awards.

Borivoje Nikolić (Senior Member, IEEE) received the Dipl.Ing. and M.Sc. degrees in electrical engineering from the University of Belgrade, Belgrade, Serbia, in 1992 and 1994, respectively, and the Ph.D. degree from the University of California, Davis, CA, USA, in 1999.

In 1999, he joined the Department of Electrical Engineering and Computer Sciences, University of California, Berkeley, CA, USA, where he is now a National Semiconductor Distinguished Professor of Engineering. His research activities include digital, analog, and RF integrated circuit design and VLSI implementation of communications and signal processing systems. He is coauthor of the book *Digital Integrated Circuits: A Design Perspective* (2nd ed., Prentice-Hall, 2003).

Dr. Nikolić received the NSF CAREER Award in 2003, the College of Engineering Best Doctoral Dissertation Prize and Anil K. Jain Prize for the Best Doctoral Dissertation in Electrical and Computer Engineering at UC Davis in 1999, as well as the City of Belgrade Award for the Best Diploma Thesis in 1992. For work with his students and colleagues, he has received the Best Paper awards at the IEEE International Solid-State Circuits Conference, Symposium on VLSI Circuits, IEEE International SOI Conference, European Solid-State Device Research Conference, European Solid-State Circuits Conference, S3S Conference, and the ACM/IEEE International Symposium of Low-Power Electronics. In 2014-2015, he was an IEEE Solid-State Circuits Society Distinguished Lecturer.

Ali M. Niknejad (Fellow, IEEE) received the B.S.E.E. degree from the University of California, Los Angeles, CA, USA, in 1994, and the Master and Ph.D. degrees in electrical engineering from the University of California, Berkeley, CA, USA, in 1997 and 2000, respectively.

He is currently a Professor with the Electrical Engineering and Computer Science Department, UC Berkeley, and Faculty Director of the Berkeley Wireless Research Center (BWRC). He is a co-founder of HMicro and inventor of the REACH technology, which has the potential to deliver robust wireless solutions to the healthcare industry. His research interests lie within the area of wireless and broadband communications and biomedical imaging.

Prof. Niknejad is the recipient of the 2012 ASEE Frederick Emmons Terman, the co-recipient of the 2013 Jack Kilby Award for Outstanding Student Paper for his work on an efficient Quadrature Digital Spatial Modulator at 60 GHz, the co-recipient of the 2010 Jack Kilby Award for Outstanding Student Paper for his work on a 90-GHz pulser with 30 GHz of bandwidth for medical imaging, and the co-recipient of the Outstanding Technology Directions Paper at ISSCC 2004 for co-developing a modeling approach for devices up to 65 GHz. In 2010-2011, he was an IEEE Solid-State Circuits Society Distinguished Lecturer.